Measurement 256 (2025) 118561

Contents lists available at ScienceDirect

Measurement

journal homepage: www.elsevier.com/locate/measurement

# Fractal and multifractal new metrics for pathological characterization and quantification in diabetic retinopathy and glaucoma

Asmae Igalla El-Youssfi *, José Manuel López-Alonso

*Optics Department, Faculty of Optics and Optometry, University Complutense of Madrid, C/ Arcos de Jalón, 118, 28037 Madrid, Spain*

ARTICLE INFO

*Keywords:*
Fractal dimension
Multifractal spectrum
Kullback–Leibler divergence
Mahalanobis distance
Diabetic retinopathy
Glaucoma

ABSTRACT

Fractal and multifractal analysis of retinal vasculature are considered as potential biomarkers to detect several vascular pathologies affecting the retina, by analysing fundus images. The use of these tools requires additional metrics that allow the quantification and characterization of the retinal image. In the present study, fractal and multifractal analysis were used to characterize images of pathological retinas classified as diabetic retinopathy and glaucoma. Using both tools, several quantitative metrics based on Kullback–Leibler divergence and Mahalanobis distance among others, were developed to quantify the severity of the pathology in each retina within the two groups. These metrics allow to give a value of the affectation of the retinal vasculature, identify all the points considered as anomalous and facilitate the classification of the retinas according to their degree of severity. The analysis allowed to distinguish between healthy and pathological retinas. In addition, with the developed metrics it has been possible to determine the affected areas of each pathological retina, determine the degree of affectation of these areas, and quantify the severity of the retina. The results were based on quantitative and qualitative measures obtained through fractal and multifractal analysis. The metrics used showed consistent agreement with the findings obtained in the study.

## 1. Introduction

The circulatory system is responsible for transporting blood and lymph through the vessels in order to supply oxygen and nutrients to the body's tissues and remove waste from the tissues [1]. The development of this system is not a random process, but rather follows a set of optimization principles, such as minimum friction between the blood flow, vessel wall and optimal heart rate to achieve adequate blood supply and distance of shorter transportation. When optimal physiological conditions are not maintained, disorders or anomalies develop in the vascular network, affecting the arteries or veins. These alterations may impair blood flow by causing obstructions, weakening vessel walls, or damaging the venous valves [2]. Therefore, many organs and body structures can be damaged by vascular disease due to the decrease or obstruction of blood flow, as occurs in conditions such as diabetes [3], high blood pressure [4] and other cardiovascular and cerebrovascular diseases [5]. These pathologies can be detected non-invasively through fundus images, which provide valuable information by allowing the analysis of the complexity of the branching pattern of the retinal vasculature [6]. In the literature there are several methods for the analysis of retinal vasculature, among which fractal and multifractal analysis stand out [7], as they are considered potential biomarker for the detection of pathologies that affect retinal vascularization and lead to vision loss [8]. Diabetic retinopathy [9] and glaucoma [10] are among the leading causes of vision loss worldwide and are both associated with vascular impairment.

Diabetic retinopathy (DR) is one of the main microvascular complications of diabetes and leading cause of vision loss worldwide, which may result in total blindness [11,12]. From a clinical perspective, DR progresses through two broad stages that correspond to Non-proliferative Diabetic Retinopathy (NPDR) and Proliferative Diabetic Retinopathy (PDR). These stages are characterized by progressive alterations of the retinal microvasculature and are classified according to the severity of the visual impairment and the characteristics of the lesions present in each stage. Microaneurysms, hard and soft exudates, haemorrhages, and macular edema are commonly observed in NPDR where the macula may become swollen due to the presence of exudates or localized fluid accumulation [13]. In the PDR stage, the pathology advances to produce abnormal neovascularization. As the disease progresses, the number of non-perfused capillaries increases, worsening

* Corresponding author.
*E-mail address:* asmaeiga@ucm.es (A.I. El-Youssfi).

https://doi.org/10.1016/j.measurement.2025.118561
Received 21 February 2025; Received in revised form 4 July 2025; Accepted 25 July 2025
Available online 25 July 2025

retinal ischemia. This process stimulates the growth of abundant new non-functional and very fragile vessels that present additional problems that can extend to the vitreous and cause haemorrhages, potentially leading to irreversible blindness [14,15].

In diabetic retinopathy, chronic hyperglycemia alters the normal vascular architecture, reducing its efficiency and damaging the capillary network, disrupting the optimal fractal pattern. Several studies have shown that lower fractal dimensions in the retina are associated with an increased risk of diabetic retinopathy and its complications [16–21]. This may be because a lower fractal dimension reflects a less complex and potentially less resilient vascular network. In healthy retinas, the vasculature displays high complexity and extensive branching, resulting in a high fractal dimension. This suggests that the retinal vasculature adheres to optimal fractal principles, enhancing the efficiency of blood flow and oxygen delivery while minimizing energy expenditure [22].

As diabetic retinopathy advances, progressive capillary damage occurs due to pathological alterations such as microaneurysms and areas of non-perfusion, which reduce the complexity of the vascular network [23–27]. The result is a more chaotic and sparsely branched vascular structure, which may manifest as a decrease in fractal dimension.

Glaucoma is a very serious, chronic, and progressive disease, and is the leading cause of irreversible blindness worldwide [28]. It is commonly associated with increased intraocular pressure, which leads to damage of the optic nerve and thinning of the retinal nerve fiber layer [29]. In addition to structural damage, glaucoma is also associated with alterations in the retinal vasculature, including changes in vascular calibre, loss of peripapillary capillary perfusion, and retinal blood flow dysfunction [30]. Although the exact mechanisms underlying these vascular changes are not yet fully understood, they represent an important and active field of research.

Glaucoma has been associated with dysfunction in ocular blood flow, particularly in the peripapillary and macular regions. A reduction in metabolic demand may occur in the affected areas, possibly linked to the loss of ganglion cells and their axons, which constitute the retinal nerve fiber layer [31,32]. This hypoperfusion could lead to a progressive loss of smaller capillaries, which in turn could reflect a decrease in the complexity and branching of the vascular network. Consequently, this may be reflected in a reduction in fractal dimension as the disease progresses. Several studies have associated a reduction in the fractal dimension of retinal vessels with nerve fiber loss in glaucomatous eyes [9,31–33].

To quantify the structural alterations observed in vascular complexity in pathological retinas, the use of mathematical tools such as fractal analysis has been motivated. Fractals are a useful tool to explain a variety of natural phenomena that exhibit some scale invariance with irregular and self-similar structures. One such example is the retinal vasculature [8]. Fractal objects have a non-integer dimension that cannot be measured using traditional Euclidean geometry [34]. Fractal dimension is used for this purpose [35].

There is a wide variety of computer algorithms to estimate different types of fractal dimension (FD), such as box-counting (the most popular), mass-radius, information dimension, correlation dimension, among others [7,35,36].

Dimension box-counting is the simplest and most widely used method to estimate the FD of fractal objects. This method consists of covering the entire space of the image the binarized fractal object with square boxes of side length ε and counting the number of boxes, N(ε), that contain any part of the object (see Fig. 1). A logarithmic plot is then constructed by plotting log $N(\varepsilon)$ against log $\varepsilon$, resulting in a linear relationship whose slope corresponds to −D, where D is the box-counting fractal dimension of the object [35,37,38].

The Local Fractal Dimension (LFD) and Connected Fractal Local Dimension (Dlc) are two types of fractal dimensions that adapt very well to the case of fractal analysis of the retinal vasculature [39,40]. Both are based on box-counting but particularized in areas around each point of the image through boxes of a certain size. For the LFD the process consists of calculating the fractal dimension with the box-counting

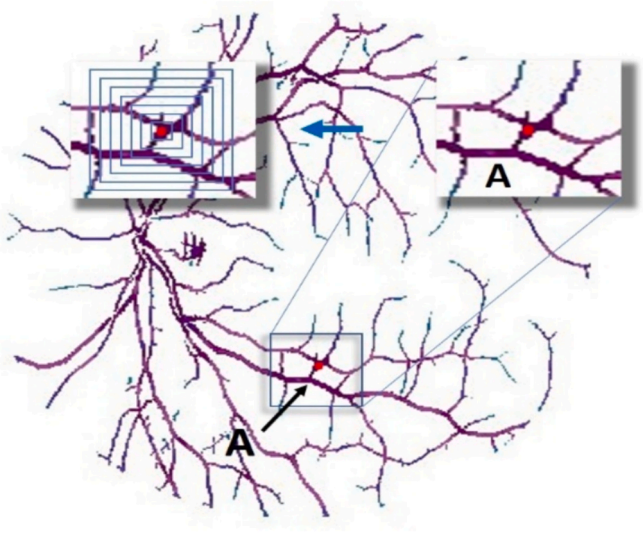


**Fig. 2.** A graphical representation of the box-counting dimension method for estimating the local connected fractal dimension. A digitized version of a retina is shown, with a box of specific size centered on a particular pixel, A. The array inside the box is extracted (the dark square marks A, the center of the box). The local connected set is shown in purple, while the unconnected pixels are blue. The number of pixels is analysed within boxes of increasing size, all centered on A.

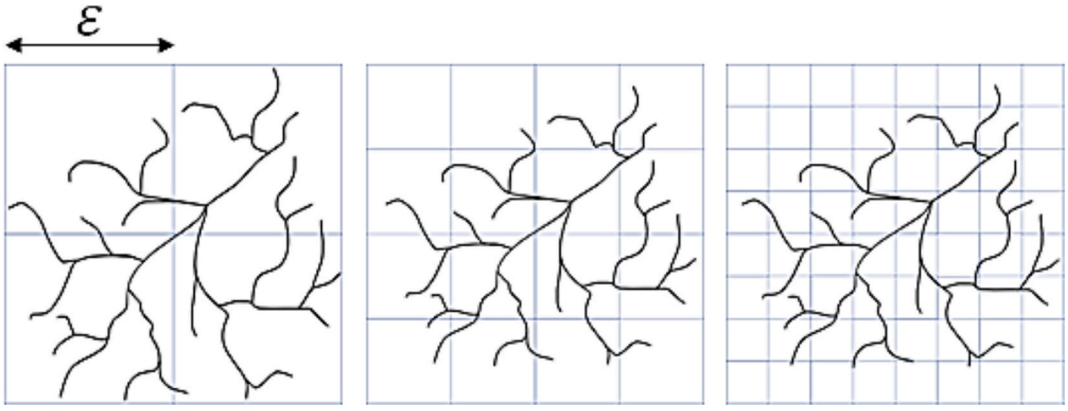


**Fig. 1.** Box-Counting dimension calculation procedure. As the number $\varepsilon$ decreases, the number N (ε) of boxes that cover the fractal object grows exponentially.

method for all points A of the image where the object exists [39,40] (see Fig. 2).

It is, therefore, a fractal dimension restricted to a local region around each point A of the object. If, instead of counting all the points within the box that surround point A, only those directly connected to A are considered, the result is more specialized measure of local fractal dimension, known as the connected local fractal dimension (Dlc) [39].

Finally, the fractal dimension is estimated by performing a linear regression of the logarithm of the number of boxes that contain part of the object, log $N(\varepsilon)$, against the logarithm of the box size, $\log(\varepsilon)$. The slope of the resulting line corresponds to the fractal dimension [41]. This measurement follows a power-law relationship, given by:

$$M(\varepsilon) = \varepsilon^{-FD} \tag{1}$$

where M(ε) represent the total mass or number of the pixels in a box of size (ε), and FD represent the fractal dimension that provides a measure of the geometrical complexity of the structure of the fractal object at different scales. Then, FD is formally estimated as:

$$FD = -\lim_{\varepsilon \to 0}\left(\frac{log(M(\varepsilon))}{log(\varepsilon)}\right) \tag{2}$$

The previous local measurements defined by the fractal dimension equation (2) shows that fractal characteristics can vary across different regions of the object. In the case of retinal vasculature, these spatial variations in fractality are better characterized by the multifractal spectrum [42]. Multifractal spectrum (MFS) is a concept used in the literature to characterize the complexity of irregular structures that exhibit variability of multiple scales, presenting different fractal in various regions of the object [43]. If in equation (2), M(ε) is divided by the total number of points of the object, a probability value is obtained for each box, which scales with its size according to FD. However, if the object is not monofractal, this probability will depend not only on the box size $\varepsilon$, but also on the location $k$ of each box. Thus, the probability scales as $P(k,\varepsilon)\ \varepsilon^{\alpha_k}$, at different locations $k$, where the exponents $\alpha_k$ are known as Hölder exponents [44]. Multifractality can then be characterized by looking at the number of boxes (or points $k$) for which the Hölder exponent is in the interval $[\alpha, \alpha + d\alpha]$. This number scales as $\varepsilon^{-f(\alpha)}$, where $f(\alpha)$ denotes the fractal dimension of the set of points characterized by the local Hölder exponent $\alpha$. The function $f(\alpha)$, when considered over the range of $\alpha$, represents the multifractal spectrum of the object [45].

The calculation of the multifractal spectrum is based on the normalized probability measure defined by:

$$\mu_k(q,\varepsilon) = \frac{P(k,\varepsilon)^q}{\sum_k P(k,\varepsilon)^q} \tag{3}$$

where $P(k,\varepsilon)$ is the probability associated with each box $k$ of size $\varepsilon$, and $q$ acts as a magnifier that modulates the influence of the regions according to their measurement density. Values of $q > 1$ highlight the high probability or denser regions of the object, while values of $q < 1$ emphasize the less dense or more dispersed regions.

From this probability measure, the singular exponents $\alpha(q)$ and the fractal dimension $f(\alpha(q))$ can be calculated, which together describe the multifractal spectrum. In this sense, $\alpha$ represents the intensity of the local singularities, while $f(\alpha)$ indicates the fractal dimension of the subset of singularities that share the same degree of irregularity $\alpha$ [46]. The multifractal spectrum reaches its maximum at the dominant singularity $(\alpha_0)$, where the value $f(\alpha_0)$ corresponds to a dominant fractal dimension that represents the most prevalent set of singularities in the structure of the fractal object. Appreciable values of the spectrum to the left $(q > 1)$ and right $(q < 1)$ of $\alpha_0$ indicate that the object is multifractal. These values reflect the presence of important fluctuations, especially in the region related to high density areas, that is, left side of the spectrum [47–49].

The multifractal spectrum is a measure that allows the characterization of complex structures with a certain degree of self-similarity, such as the retinal vasculature. In this sense, the vessels possess a certain degree of local irregularity (irregularity understood as a certain tortuosity, indistinct branching patterns, and structural variability), which is characterized by the parameter α, which exhibit spatial variability. The value f (α) measures the fractal dimension of the points in the vasculature with the same α. Therefore, a large range between the maximum and minimum values of regularity is indicative of wide multifractal spectrum, meaning that the structure contains a high number of different types of irregularities in the structure, hence the word multifractal. Since an irregular line will tend to have lower Hölder exponents [44], the increase in irregularities is typically reflected as a greater width on the left side of the multifractal spectrum (see Fig. 6). Pathology such as diabetic retinopathy produces irregular blood vessels, which are expected to exhibit a stronger multifractal behaviour than healthy retinas, due to a greater variety of local irregularities. Similar behaviour may occur in other pathologies, making the characterization of the multifractal spectrum's width potentially important for distinguishing healthy from pathological retinas.

This study initially focuses on identifying between healthy and pathological retinas, specifically those affected by diabetic retinopathy and glaucoma based on the analysis of their vasculature using the fractal and multifractal analysis. Subsequently, the affected regions that show characteristics distinctions between healthy and diseased retinas are determined, and the retinas are classified into different degrees of vascular involvement using quantitative metrics specifically developed for this purpose.

Although there is currently no validated reference scale for this vascular-based classification, this proposal is presented as a methodological exploration. Its value lies in providing objective and measurable criteria for assessing retinal vascular status. These metrics could facilitate more detailed monitoring of disease progression, support clinical decision-making, especially in stages where conventional signs are not yet evident, and enrich the understanding of pathologies such as glaucoma, whose etiology is not yet fully defined but in which vascular involvement is suspected. The paper is structured as follows: after introduction, a section on materials and methods is presented. Next, the main results for each pathology are presented and it ends with a discussion and main conclusions, in addition to the bibliographic references consulted.

## 2. Material and methods

### 2.1. Dataset

A public dataset High-Resolution Fundus (HRF) was used in this study. HRF dataset can be downloaded from a public website of the Pattern Recognition Lab of the Friedrich Alexander Technical University Erlangen-Nürnberg [50]. This dataset contains 45 colour retinal images (24 bits – RGB) classified into healthy and pathological retinas. The images are divided into two groups: the first group includes 15 images of healthy retinas, the second group corresponds to pathological images, subdivided into 15 images of diabetic retinopathy (DR) and 15 images of glaucomatous retinas. These images have a size of 2336 × 3504 pixels and were captured by a CANON CF-60 Uvi mydriatic retinograph using a "Canon EOS 20D" type camera. This dataset also provides manually segmented (Gold Standard) images corresponding to each RGB image (with identical dimensions), as well as binary masks that delimiting the retina and the surrounding black background, thus defining the field of view (FOV).

Pathological retinas in the HRF dataset, both DR and glaucoma, are not classified by degree of severity. In the case of DR, they are not differentiated between mild, moderate, severe (NPDR), or advanced cases PDR.

According to Odstrcilik et al. [51] explain that within each group of

pathological retinas in the HRF dataset, pathological changes are observed in the retinas such as haemorrhages, neovascularization, bright lesions and scars from laser treatment in the case of the DR group. For the case of retinas with glaucoma, they mention that the retinas correspond to cases in an advanced stage, with focal and diffuse loss of the nerve fibre layer. Although these observed pathological changes could be useful for the classification of the retinas, especially in the case of DR, a classification is not provided that indicates the degree of severity of each retina. Therefore, studying the whole group of unclassified pathological retinas of different degrees of severity can provide information, but it is insufficient to understand the progression of the pathology or determine the appropriate treatment. In this sense, in the following sections of this study, metrics are developed that allow a classification of pathological retinas, based on the fractal and multifractal analysis of the retinal vasculature.

All images have been analysed on a computer with a 2.40 GHz processor and 16 GB RAM with the software MATLAB version: 9.13.0 (R2022b) and ImageJ [52,53].

## 2.2. Methodology

### 2.2.1. Software and parameters for fractal analysis

Previous studies by the same authors have shown that certain retinal vasculature segmentation methods can significantly influence fractal and multifractal analysis [40]. Some of the metrics used in the present work were also employed in that context to assess such effects. For this reason, in order to avoid any bias introduced by segmentation in the estimation of the fractal dimension and the multifractal spectrum, and to more accurately characterize pathological retinas, it was decided to directly use images manually segmented by experts available in the same HRF dataset.

This approach ensures more accurate measurements and enhances the reliability of the pathological characterization. Since the images have a high resolution (2336 × 3504 pixels), their fractal analysis required significant memory and processing time.

In this regard, different resolution reduction factors (25 %, 50 %, and 75 %) were evaluated with the aim of optimizing the performance of the analysis algorithms and improving the visualization of the affected areas of the retinal vasculature. As shown in Table 1, which presents the times required to process and analyse the retinal vasculature using FracLac, a plugin for the National Institutes of Health (NIH) ImageJ software [54], a reduction factor of 0.25 (75 %) was determined to provide an adequate balance between accuracy and efficiency. This reduction significantly accelerated the calculations, avoided software crashes, and improved processing stability without compromising the quality of the fractal analysis.

To reduce the size of the retinal images, the MATLAB *imresize* function was used, which employs different interpolation methods that allow images to be scaled efficiently. In this case, the bicubic interpolation method was used to calculate the new pixels values using the 4 × 4 neighbourhood technique (16 pixels closet to the target pixel). This method preserves image detail by producing smoother transitions and avoids visual artifacts (such as aliasing) more common in simpler methods such as nearest neighbour. In this way, the reduction in image size does not significantly compromise the effective resolution of the retinal vasculature, thus preserving the morphological structure essential for fractal and multifractal analysis.

**Table 1**
The time required to perform the fractal analysis of the 45 retinal images in the HRF dataset according to the image size.

| Resampling factor | Retinal Image Size (pixels) | Time required for fractal analysis (s) |
|---|---|---|
| 0 % | 2336 × 3504 | 21,600 |
| 25 % | 1752 × 2628 | 8100 |
| 50 % | 1168 × 1752 | 2700 |
| 75 % | 876 × 584 | 600 |

The process that follows the reduction of the retinal image consists of entering the manually segmented image of the retina, selecting the region of interest (ROI) of the retina, and using FracLac. Within FracLac it is selected the Dlc option to measure the local fractal dimension (LFD) and the connected local fractal dimension (Dlc) which are based on the box-counting method. The method must yield a minimum and maximum dimension value of the box. In this case, the minimum value for the box size has been set to 1 pixel and the maximum value to 31 pixels, since these values are commonly used in similar studies and are in agreement with the ranges adopted in previous works reported in the specialized literature on fractal and multifractal analysis of retinal and biomedical images [41,55,56]. This analysis returns a retinal image with each point of the retinal vasculature analysed with the FracLac, with an intensity proportional to its local and connected local fractal dimension (see Fig. 3), and a table of values of the Dlc and LFD of each point of the retinal vasculature. For the multifractal spectrum, the multifractal (MF) analysis option is selected for values of $q[-30, 30]$ [49], and this analysis provides a table with the data for $\alpha$ and $f(\alpha)$ as a function of each value of $q$. For both analyzes a binarized image is required to carry out the process, therefore, ImageJ automatically converts the segmented input image into a binary image. This process applies to all images.

### 2.2.2. Analysis of probability distributions of fractal parameters

The data obtained from the fractal and multifractal analysis are used to generate the probability distributions of the FD for each image within the retinal groups, as well as the multifractal spectrum of the retinal vasculature. This allows to study the fractal behaviour of the retinal vasculature in healthy retinas compared to pathological retinas, with the aim of identifying the differences between them, determining the specific regions where the differences occur, and quantifying their extent, defined as degree of affectation (AD).

To clearly distinguish between different types of retinas (healthy, DR and glaucoma) it is important to use parameters that are characteristic and stable for retinas of the same group. In this sense, the probability distributions of the fractal dimension $pdf_g(FD)$ are used, with FD being both the LFD and the Dlc and $g$ being the group of retinas considered (15 for healthy, 15 for DR and 15 for glaucoma). The stability of these parameters for each group will be measured using a noise signal for each value of $x_{FD}$, $SNR(x_{FD})$ defined as

$$SNR(x_{FD}) = \frac{\langle pdf_g(x_{FD})\rangle_g}{\sigma\left(pdf_g(x_{FD})\right)_g} \tag{4}$$

where the mean and standard deviation are taken from the probability distribution function (pdf) of each group $g$ in the value $x_{FD}$. This SNR parameter helps to choose what type of fractal dimension can be calculated with less relative error and, therefore, may be more useful for discriminating between groups of retinas.

A second method is used to quantify whether the differences between the probability distributions of two groups of retinas are statistically significant. To do this, and for each value of the considered FD, $x_{FD}$, the following pairs of data vectors are taken. $\left[pdf_{g_{i_1}}(x_{FD}), \cdots pdf_{g_{i_n}}(x_{FD})\right]$, $\left[pdf_{g_{j_1}}(x_{FD}), \cdots pdf_{g_{j_n}}(x_{FD})\right]$, being $g_{i_{1\cdots n}}, g_{j_{1\cdots n}}$ the retinas of the group $g_i$ and $g_j$ taken from $i, j = 1, \cdots n(=15)$ for the retinas within each group. A *Wilcoxon* rank-sum test [57] is then applied for the statistical significance of the difference between the two groups ($p < 0.05$) and the *p-value* is represented as a function of $x_{FD}$. Points where $p < 0.05$ indicate that the difference between the probability distributions for the two groups is statistically significant. The Wilcoxon rank-sum test is a non-parametric statistical test that assesses whether the medians of two independent samples are statistically different and determines whether the observed difference can be attributed to chance. This test returns a *p-*

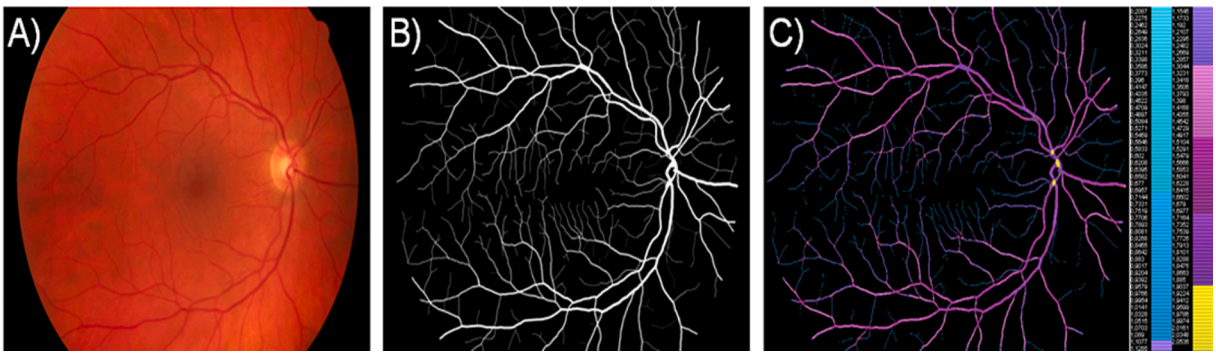


**Fig. 3.** (A) The original colour image of a retina from the HRF dataset (584 × 876 × 3 pixels). (B) The manually segmented image of the same retina from the HRF dataset. (C) Fractal analysis of the retina with FracLac. The colours represent the value of the fractal dimension from light blue (0 FD) to yellow (2 FD), passing through average values of 1.5 in violet (1.5 FD).

*value*, which is interpreted as follows: if $p < 0.05$, the null hypothesis is not rejected (the distributions are equal); if $p < 0.05$, the null hypothesis is rejected, indicating a statistically significant difference between the groups [57].

From this method, two parameters quantifying the difference are defined. The first, a degree of differentiation between points (DDP) as the percentage of the definition domain of the pdfs considered where the statistical difference is significant. The second is the average value of all *p-value* $< 0.05$ $(\ln(p) = -2.99)$, denominated $\overline{p_{sig}}$ [40].

The third method used consists of quantifying the degree of the retinal vasculature anomaly based on the Kullback-Leibler $(D_{KL})$ divergence between the probability distributions of the fractal dimensions of the pathological retinas compared to the healthy ones [58]. The $D_{KL}$ is an asymmetric measure between two probability distributions "Q" and "P", and is expressed with the following equation:

$$D_{KL}(P\|Q) = \int P(x) log\left(\frac{P(x)}{Q(x)}\right) dx \tag{5}$$

$Q$ being a reference probability distribution, and $P$ being another one whose divergence from the $Q$ distribution is to be measured.

This measure is used to measure the divergence between the probability distributions of the FD of healthy retinas, which is represented as the reference distribution $Q$, and the probability distributions of the FD of pathological retinas, which is taken as the distribution $P$.

The use of this divergence consists of measuring for each distribution of group $Q$ its divergence $D_{KL_Q}$ with respect to the mean of the whole reference group $Q$, where a mean value and an uncertainty given by standard deviation of this divergence $(\overline{D_{KL_Q}} \pm \sigma(D_{KLQ}))$, is obtained. This value, $\overline{D_{KL_Q}}$, is the normalization value that is used to calculate the divergence $D_{KLN}$ normalized from the other pathological group $P$ as $D_{KL_N} = \frac{D_{KLP}}{\overline{D_{KL_Q}}}$, being, $D_{KL_P}$, the divergence of a distribution $P$ with respect to, $\overline{D_{KL_Q}}$, without normalizing (see Fig. 4).

For this $D_{KL_N}$ value, an uncertainty is also calculated through the uncertainty $\sigma(D_{KL_Q})$ of the $\overline{D_{KL_Q}}$ of the reference group, and it is obtained that:

$$\sigma(D_{KL_N}) = D_{KL_N} * \left(\frac{\sigma(D_{KL_Q})}{\overline{D_{KL_Q}}}\right) \tag{6}$$

The values of the $D_{KL_N}$ together with their uncertainty $\sigma(D_{KL_N})$, are used to characterize and quantify the degree of divergence of the FD of the vasculature in each pathological retinas with respect to healthy retinas, according to one of the following criteria:

- When $D_{KL_N} - \sigma(D_{KLN}) > 1$, the retinal distribution under comparison shows clear divergence and therefore considered pathological.

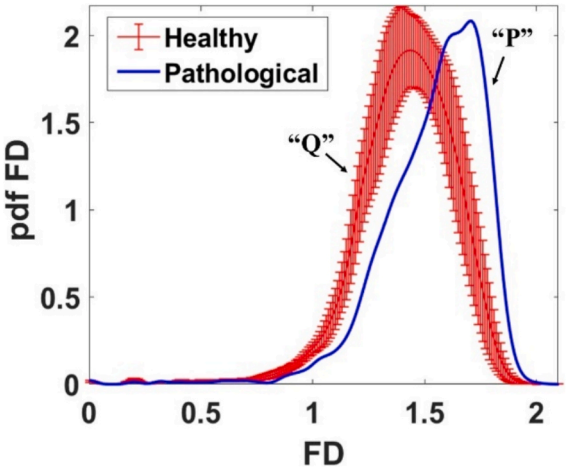


**Fig. 4.** The graphical representation of the Kullback-Leibler divergence between the mean distribution of healthy retinas $Q$ and a pathological retina $P$.

- In the opposite case of the previous rule, when $D_{KL_N} + \sigma(D_{KLN}) < 1$, the retinal distribution under comparison is not divergent and is therefore considered healthy.
- When none of the above criteria are met, the retinal case is classified as doubtful.

To assess the reliability of the characterization and quantification of the pathological retinas using the $D_{KLN}$ measurements, a normalized reliability divergence $D_{KL_R}$ is calculated at a 95 % confidence level, ensuring compliance with the above criteria, using the following equation:

$$D_{KL_R} = \frac{1}{1 + 2*\left(\frac{\sigma(D_{KL_Q})}{D_{KL_Q}}\right)} \tag{7}$$

therefore, all $D_{KL_N} \pm \sigma(D_{KL_N})$ measurements exceeding $D_{KL_R}$ are classified as pathological cases, with clearly significant divergence.

The fourth method to characterize the pathological retinal images consisted of developing an algorithm in the MATLAB platform that calculates and represents the mean probability distribution and the standard deviation (STD) of the control group (healthy retinas). This reference group is used to compare with the probability distributions of the FD of each pathological retina.

The next step of the algorithm involves analysing the pathological retinas individually, starting with those affected by diabetic retinopathy. For each retina, the probability distribution of the FD is calculated and plotted, and the compared with the mean probability distribution and

standard deviation of the FD from the control group.

The algorithm then calculates all the points of the FD probability distribution of each pathological retina analysed and identifies those that differ from the mean probability distribution ± STD of the control group. The points of the FD probability distribution of the pathological retina that differ significantly from the mean probability distribution ± STD of the control retinas (above or below the standard deviation of the control group) are identified as anomalous points that are used to calculate the degree of affection of the vasculature of the pathological retina. The anomalous points can represent low or high FD. To identify the areas to which the points identified as anomalous belong, the fractality distribution is divided into two intervals to describe the region of involvement of each case. The first interval, [0, 1.5], corresponds to the low-fractality zone (low-F), while the second, [1.5, 2], represents the high-fractality zone (high-F) (see Fig. 5).

For points identified as abnormal, a binary mask is created to select those areas of the retinal vasculature outside the normal range. For each abnormal region, the area covered by these points is calculated relative to the total retinal vasculature area, representing the AD (%) of that specific region.

### 2.2.3. Metrics for characterizing multifractal spectra

Several metrics were used for the characterization of multifractal spectra [49]. These metrics aim to analyse the differences between the mean spectrum of the control group (healthy retinas) and those of the DR and Glaucoma groups, in order to determine the multifractal behaviour within each of the three retinal groups. The multifractal spectra are represented by the values of α and f(α) and are calculated based on the magnifying parameter $q$. The multifractal spectra are characterized not only by $\alpha_0$ and $f(\alpha_0)$, but also by several other parameters derived from α and f(α) to describe the spectrum more comprehensively. These parameters include $\alpha_0$, the dominant singularity; the asymmetry A between both indices of the spectrum which is calculated as $A = \frac{\alpha_0 - \alpha_{min}}{\alpha_{max} - \alpha_0}$; the spectral divergence or the width of the singularity strength, $\Delta\alpha = \alpha_{max} - \alpha_{min}$; the height of the left side of the spectrum, $\Delta f_1 = f_{max} - f_{min}$; and the dominant fractal dimension $f(\alpha_0)$, which coincides with $D_0 = f_{max}$ (see Fig. 6) [47,49].

Other parameters descriptor parameters of the multifractal spectrum have been defined. These include $\Delta\alpha_1 = \alpha_0 - \alpha_{min}$, and $\Delta\alpha_2 = \alpha_{max} - \alpha_0$, which represent the width of the left and right sides of the multifractal spectrum, respectively; $\Delta f_2 = f_{max} - f(\alpha_{min})$, representing the height of the right side of the spectrum; and $l_1 = \sqrt{(\Delta\alpha_1)^2 + (\Delta f_1)^2}$, and $l_2 = \sqrt{(\Delta\alpha_2)^2 + (\Delta f_2)^2}$, which correspond to the length of the left (multifractal) and right (monofractal) sides of the multifractal spectrum, respectively. These ten parameters were used to characterize the multifractal spectra of the pathological retinas using a metric, defined as Metric Distance 1 (MD1) [49].

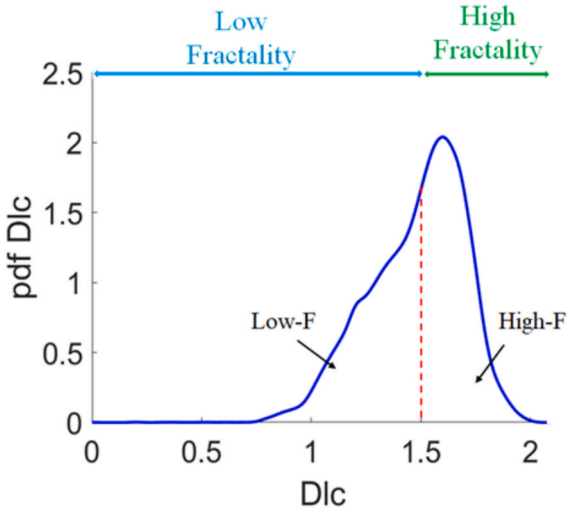


**Fig. 5.** Graphical representation of the division of the probability distribution of the FD (Dlc) into two ranges: Low Fractality (Low-F), covering the interval [0, 1.5], and High Fractality (High-F), covering the interval [1.5, 2].

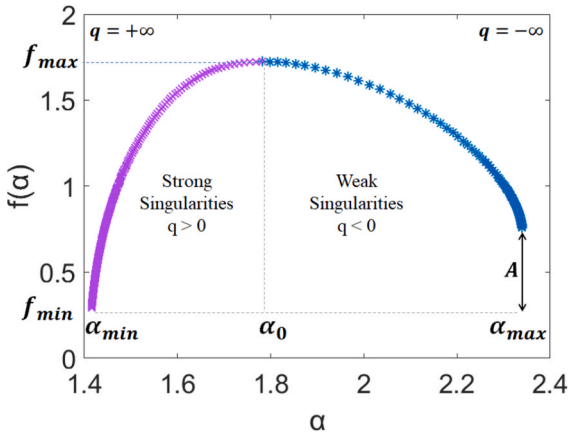


**Fig. 6.** Representation of the descriptive characteristic parameters of multifractal spectra.

This metric provides a numerical measure of the distance between the spectrum of the pathological retina and the average spectrum of healthy retinas, based on the descriptor parameters $[\alpha_0, \Delta\alpha, f(\alpha_0), \Delta f_1, \Delta f_2, \Delta\alpha_1, \Delta\alpha_2, l_1, l_2, A]$.

In this case, a vector is defined for each retina $i$ in the reference group of healthy retinas as $V_{r,i} = [\alpha_0, \Delta\alpha, f(\alpha_0), \Delta f_1, \Delta f_2, \Delta\alpha_1, \Delta\alpha_2, l_1, l_2, A]$. The reference group $R$ is then characterized by the average vector given as: $V_R = \left(\frac{1}{N}\right)\sum_{i=1}^{N} V_{r,i}$, where $N$ is the total number of retinas in the reference group. For each retina in this group, the MD1 is calculated as:

$$d_{R,i} = \sqrt{(V_{r,i} - V_R).(V_{r,i} - V_R)^T} \tag{8}$$

Then, for this reference group, a mean distance $\langle d_{R,i}\rangle$ is calculated, which is used as a normalization value to normalize the MD1 of each pathological retina.

For the DR and glaucoma groups, another vector $V_{n,i}$ is defined for each retina $i$ belonging to group $n$. Using these vectors, a distance $d_{n,i}$ is calculated as:

$$d_{n,i} = \sqrt{(V_{n,i} - V_r).(V_{n,i} - V_r)^T} \tag{9}$$

The distance $(d_{n,i})$ is normalized by dividing it by the mean distance $\langle d_{R,i}\rangle$ of the control group. The distance between the spectrum of a retina of the group "$n$" and the reference group "$R$" is given by:

$$d(n,R) = \frac{d_{n,i}}{\langle d_{R,i}\rangle} \tag{10}$$

Therefore, a distance $d(n,R) > 1$ is interpreted as "pathological retina". Its value indicates how many times the distance of the pathological multifractal spectrum of the pathological retina respect to $V_r$ differs from the mean distance in the reference group, with $n$ being a pathological retina (DR or glaucoma). Then, the distance MD1 can be used as a quantifier of pathology degree. For each pathological retina in the analysed groups, the distance between its multifractal spectrum and the mean spectrum of the reference is calculated. This distance is represented as $d(DR_i, R)$ in the case of DR retinas, and $d(G_i, R)$ for retinas with glaucoma, where $i$ represents each retina belonging to the DR or glaucoma groups.

A second metric, based on the Mahalanobis distance, is used to compare the descriptive parameters of the multifractal spectra of the

pathological retinas with those of the healthy retinas [49]. The Mahalanobis distance is a distance between two points in a parameter space that takes into account the covariances between them. It intuitively measures the Euclidean distance between them but normalized by the standard deviation in the considered direction. In this concrete application, this metric distance 2, denoted as MD2, is calculated from the set of spectra of the control retinas $R$. The parameters of each spectrum $r$ are represented by a vector $V_{r,i} = [\alpha_0, \Delta\alpha, f(\alpha_0), \Delta f_1, \Delta f_2, \Delta\alpha_1, \Delta\alpha_2, l_1, l_2, A]^T$, for the multifractal spectrum of the retina $i$ belonging to the control group $R$. The Mahalanobis distance is defined as:

$$D_{R,i} = \sqrt{(V_{r,i} - V_R)^T \bullet [S_r]^{-1} \bullet (V_{r,i} - V_R)} \tag{11}$$

$V_R$ being the mean vector across all spectra $r$ which is given as $V_R = \left(\frac{1}{N}\right)\sum_{i=1}^{N} V_{r,i}$, where N is the number of retinas in the control group. $S$ is the covariance matrix between parameters $[\alpha_0, \Delta\alpha, f(\alpha_0), \Delta f_1, \Delta f_2, \Delta\alpha_1, \Delta\alpha_2, l_1, l_2, A]$, across spectra "$r$". Then, a mean Mahalanobis distance $\langle D_{R,i}\rangle$ is calculated to normalize the distance of the pathological retinas.

For the spectra of each pathological retina, the Mahalanobis distance is measured through $V_{p,i}$, relative to the mean vector of the control group. Here, $V_{p,i} = [\alpha_0, \Delta\alpha, f(\alpha_0), \Delta f_1, \Delta f_2, \Delta\alpha_1, \Delta\alpha_2, l_1, l_2, A]^T$ is a vector of the descriptive parameters corresponding to each pathological spectrum, where $p$ represents a DR or glaucoma retina. The Mahalanobis distance of these pathological retinas is defined as:

$$D_{p,i} = \sqrt{(V_{p,i} - V_r)^T \bullet [S_r]^{-1} \bullet (V_{p,i} - V_r)} \tag{12}$$

The $D_{p,i}$ value of each pathological retina is normalized with the $\langle D_{R,i}\rangle$ value of the healthy retinas as:

$$D_{(p,i)_N} = \frac{D_{p,i}}{\langle D_{R,i}\rangle} \tag{13}$$

where $D_{(p,i)_N}$ is the normalized Mahalanobis distance of each pathological retina. Then, the Mahalanobis distance between the pathological group "$p$" and the control group "$R$" is obtained as:

$$D(p,R) = \langle D_{(p,i)_N}\rangle \tag{14}$$

A distance $d(p_i, R) > 1$ reflects the degree to which the multifractal spectrum of the pathological retina differs from the reference group.

A third metric was defined in this study to compare the two characteristic parameters of the multifractal spectra, α and f(α), of each retina. This metric is denoted as "MD3". As explained in the introduction, these parameters are calculated based on the magnifying parameter q, for certain values over the range $q \in [-30,30]$. This metric enables the identification of regions within the multifractal spectrum of the pathological retinas that differ significantly from of those of the control group.

With this metric each spectrum is characterized by a vector $V_q = [\alpha(q), f(\alpha(q))]$, which defines a 2D variable with a covariance matrix $S_q$, computed for each considered group of spectra of the control group, DR and Glaucoma. A mean vector of the control group is defined as: $V_q^C = \left(\frac{1}{N}\right)\sum_{i=1}^{N}(\alpha_i(q), f_i(\alpha(q)))$, where N is the number of spectra in the control group. Therefore, the control group will have a covariance matrix $S_q^C$. For pathological retinas, the Mahalanobis distance is calculated for each spectrum of each retina $i$ within a given group $p$, and for each point $q$ of the spectrum. This distance is expressed as [49]:

$$\Omega_q^{p,i} = \sqrt{\left(V_q^{p,i} - V_q^C\right)^T \bullet \left[S_q^C\right]^{-1} \bullet (V_q^{p,i} - V_q^C)} \tag{15}$$

This metric measures the distance between each $q$ value of the spectrum and the mean value of the control group and normalizes it by the standard deviation of the data in the direction of the vector considered $V_q^{p,i}$. This distance from a pathological group $p$ to the control, $\Omega_p(q)$, and is defined as:

$$\Omega_p(q) = \langle \Omega_q^{p,i}\rangle_i \tag{16}$$

This distance provides information on the most significant variations in the spectrum. Specifically, it allows determining whether the greatest variations are present in the left side of the spectrum ($q > 1$), or the right side ($q < 1$). To determine whether the differences between the Mahalanobis distances of the control group and the pathological groups are significant, the *Kruskal-Wallis* test is applied [59].

The Kruskal-Wallis test is a nonparametric test used to compare whether there are significant differences between the medians of three or more groups of independent samples. The test involves transforming the data into ranges and assessing whether the distribution of these ranges varies between the groups. The test returns a *p-value* indicating whether the distributions of all groups are equal (*p-value* $> 0.05$, the medians do not show significant differences), or whether there are statistically significant differences between at least two groups (*p-value* $< 0.05$, the medians differ) [59].

Then, this test is used to determine whether there are significant differences in the parameter $\alpha(q)$ when comparing it between the healthy group and each of the pathological groups as a function of $q$. Subsequently, the same procedure is applied to the parameter $f(\alpha(q))$. The aim is to determine which of the two parameters $\alpha(q)$ or $f(\alpha(q))$ best distinguishes between the different groups of retinas.

## 3. Results

In this study, 45 retinal images classified into healthy, DR, and glaucoma retinas are used to characterize the retinal vasculature through fractal and multifractal analysis. The results of the mean probability distribution of the Dlc and LFD of the DR and Glaucoma group compared to the healthy retina group are shown in Fig. 7. In this figure, a difference can be observed between the probability distributions of the mean FD for the glaucoma group (green), the group DR (red), and the healthy group (blue), in both Dlc and LFD representations. The mean probability distributions for the DR and glaucoma are shifted to the left, towards smaller FD values compared to the healthy retinas. This suggests that the retinal vasculature of the pathological retinas (DR and glaucoma) presents lower fractal dimensions than the control group.

To determine the most suitable FD measurement method for characterizing pathological retinas, the SNR was calculated in both methods (Dlc-LFD) (see Fig. 8). As shown in Fig. 8, healthy retinas exhibit a high SNR with both methods, indicating that either Dlc or LFD can be used indifferently in this group. However, for the DR and glaucoma groups, the LFD measurement method shows a higher SNR in both groups, with a slightly greater difference observed in the DR (see Fig. 8).

To visualize the differences between the two methods for measuring the FD of the retinal vasculature, the vasculature is reconstructed based on the Dlc and LFD values obtained at each point of the retinal vasculature. Three cases of healthy retinas, DR and glaucoma are represented in Fig. 9. In this figure, a greater uniformity in the measurement of the FD using the LFD method is observed, especially in DR and glaucoma retinas. This is because the Dlc method considers the terminal points of several vessels as isolated structures (see Fig. 9), assigning them lower FD values, which may lead to misleading interpretations.

A method based on the Wilcoxon rank-sum test has been used to support previous findings and to determine which method is more accurate. For each value of the fractal dimension, the probability density values (pdf) across all healthy retinas are compared with those pathological retinas. This allows identifying the specific FD values at which the two groups significantly differ. This method provides a degree of difference between the points (DDP) and the value of $\overline{p_{sig}}$ that determines the significance of the difference between both groups. The results of the Wilcoxon rank-sum test are represented in Fig. 10.

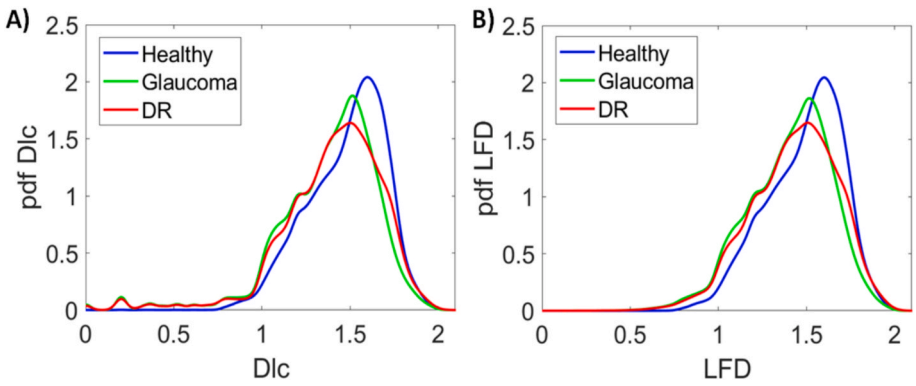


**Fig. 7.** (A) Mean probability distributions of Dlc of healthy (blue), glaucoma (green) and DR (red) retinas. (B) Mean probability distributions of LFD of healthy, glaucoma and DR retinas.

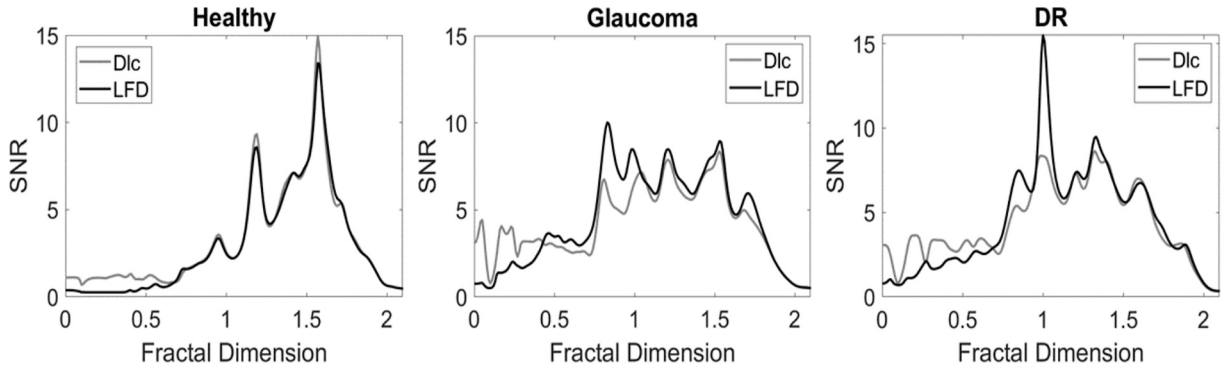


**Fig. 8.** Signal-to-noise ratio (SNR) representation between the mean probability distributions of Dlc and LFD in healthy, glaucoma and DR retinas.

In Fig. 10.A it can be observed that the mean probability distributions of the Dlc of the DR group differ from the control group by 77.25 % with a $\overline{p_{sig}}$ of 0.0037. In contrast, the difference is slightly higher for the LFD method, showing a difference of 85.78 % and a $\overline{p_{sig}}$ of 0.0039 (see Fig. 10.B) (see Table 2).

In the case of glaucoma, it is observed that for the Dlc method, the difference is 84.83 % with a significance level $\overline{p_{sig}}$ of 0.0034 (see Fig. 10.C), while for the LFD method this difference is slightly higher, similar to the DR, showing 88.15 % with a significance level of 0.0025 (see Fig. 10.D). These results, together with those obtained in the signal–noise ratio and the vessel representations based on both FD measurement methods (Dlc and LFD), led to the selection of the LFD method as the most precise option for the characterization of pathological retinas. In addition, this method is one of the most widely used in the literature [39,55,60–62]. Using LFD, the normalized Kullback-Leibler distance ($D_{KL_N}$) was calculated of each of the pathological retinas. The results for the DR retinas are presented in Table 3, and glaucoma in Table 4.

Based on these results, three retinas with different levels of $D_{KL_N}$ are selected and classified into three categories: mild, moderate and severe. These cases are used to represent the areas of the vasculature identified as abnormal in each retina. Additionally, the degree of affectation (AD) of each identified area is provided.

In the case of DR, the retina dr11 was selected as a mild case, with a $D_{KL_N} \pm \sigma(D_{KL_N})$ value of 2.15 ± 1.17. In Fig. 11. A, the LFD probability distribution of this retina is represented in comparison with the mean probability distribution and standard deviation of the LFD of healthy retinas.

In addition, all the points identified as anomalous in the vasculature of the dr11 retina are represented, and the AD value of each detected area is provided. In this case, the LFD probability distribution curve of the dr11 shifts to the left, towards the low fractality (Low-F). This may indicate a slight increase in the microvessels associated with low fractality compared to healthy retinas. This area presents an AD of 17.8 % of the total area of the retinal vasculature analysed. Furthermore, a reduction is observed in the main vessels, both veins and arteries, which correspond to the high fractality (High-F). This affectation is quantified with an AD of 23.7 %.

According to the results obtained from the distance $D_{KL_N}$, the retina dr13 was selected as a moderate case of DR, presenting a value of $D_{KL_N} \pm \sigma(D_{KL_N}) = 3.43 \pm 1.86$. The characterization results for this retina are presented in Fig. 11.B, where the LFD distribution also shifts to the left towards the low fractality region (Low-F). Like the previous case, there appears to be a slight increase in the microvessels associated with low-F compared to healthy retinas. The degree of affectation in this area is 14.6 %. The vessels representing high fractality (high-F) show a greater decrease, with an AD of 19.8 %.

For a severe case, dr1 was selected, with $D_{KL_N} \pm \sigma(D_{KL_N}) = 5.10 \pm 2.77$, and the results are represented in Fig. 11.C. As with the previous cases, dr1 also presents an increase in vessels with low-F with (AD of 15.5 %) and a decrease in vessels representing high-F (AD of 14.8 %). Therefore, in the three cases of DR, regardless of severity, it is observed that the vessels with low-F (microvessels and capillaries) increase and the number of vessels with high-F (main vessels) decreases, presenting different levels of AD in each case.

In the case of glaucoma, three retinas with different degrees of $D_{KL_N}$ were also selected and classified as mild, moderate, and severe. For the mild case, retina g12 was selected, which presents a value of $D_{KL_N} \pm \sigma(D_{KL_N}) = 3.36 \pm 1.83$. In Fig. 12.A. it can be observed that the LFD probability distribution of this retina shifts slightly towards low fractality. This indicates a slight increase in the number of vessels with low fractality and a decrease in the number of vessels with high fractality.

These areas present an AD of 18.4 % and an AD of 15.2 %, respectively. In the moderate case, retina g8 was selected, which shows a value

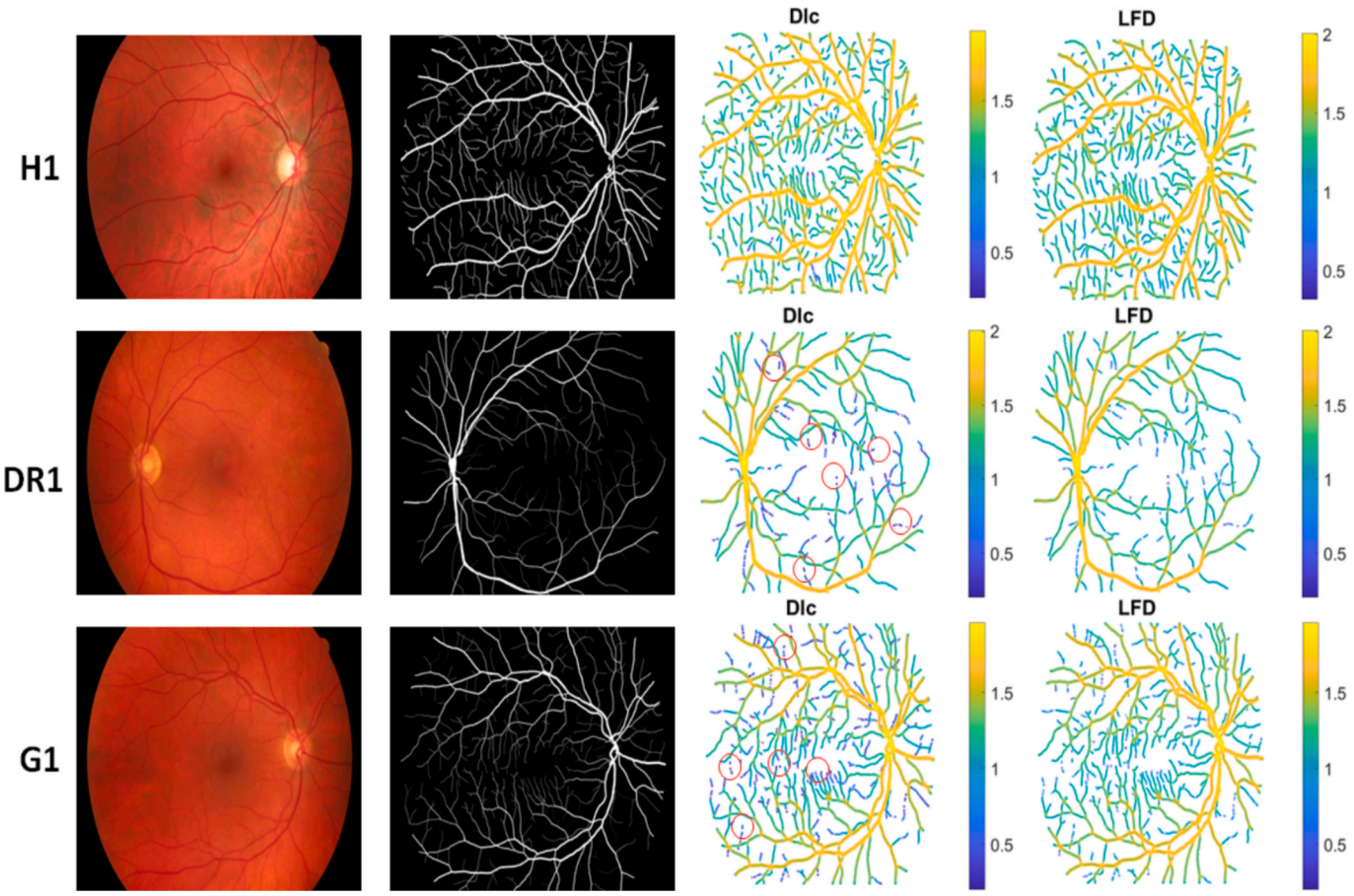


**Fig. 9.** Representation of the retinal vasculature for three cases of retinas (H1: healthy retina; DR1: Diabetic retinopathy; and G1: Glaucoma) using the Dlc and LFD values obtained in the FracLac, together with its manual segmented image and the original image in RGB.

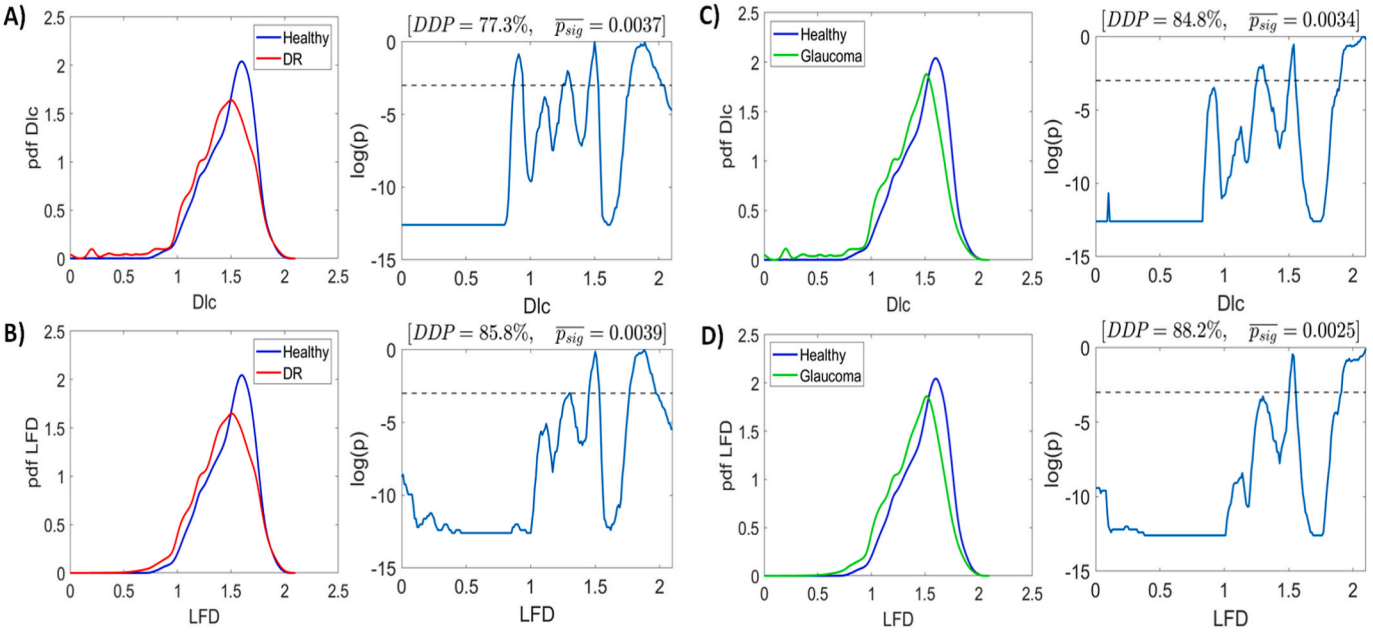


**Fig. 10.** (A) Representation of the mean probability distributions of the Dlc (A), and LFD (B) of healthy (red) and DR (red) retinas (left) and the Wilcoxon rank-sum test to determine the DDP and the $\overline{p_{sig}}$ between both groups of retinas. Comparison between healthy (red) and glaucoma (green) retinas are represented in C) for Dlc and D) for LFD.

**Table 2**
Results of the Wilcoxon rank-sum test showing the degree of significant difference between points (DDP) in the probability distributions of Dlc and LFD, with the mean $\overline{p_{sig}}$, comparing healthy retinas with DR and glaucoma.

| | Healthy vs DR | | Healthy vs Glaucoma | |
|---|---|---|---|---|
| | *DDP*(%) | $\overline{p_{sig}}$ | *DDP*(%) | $\overline{p_{sig}}$ |
| **Dlc** | 77.25 | 0.0037 | 84.83 | 0.0034 |
| **LFD** | 85.78 | 0.0039 | 88.15 | 0.0025 |

**Table 3**
The results of the $D_{KL_N} \pm \sigma(D_{KL_N})$ measurement between the LFD probability distributions of the DR retinas from the HRF dataset and the mean probability distribution of the healthy retinas from the same dataset.

| $D_{KL_N} \pm \sigma(D_{KL_N})$ | | | | | |
|---|---|---|---|---|---|
| **dr1** | 6.40 ± 3.47 | **dr6** | 3.48 ± 1.89 | **dr11** | 2.15 ± 1.17 |
| **dr2** | 5.93 ± 3.22 | **dr7** | 2.23 ± 1.21 | **dr12** | 3.54 ± 1.92 |
| **dr3** | 3.66 ± 1.99 | **dr8** | 2.74 ± 1.49 | **dr13** | 3.43 ± 1.86 |
| **dr4** | 3.29 ± 1.79 | **dr9** | 3.49 ± 1.89 | **dr14** | 2.22 ± 1.21 |
| **dr5** | 6.83 ± 3.71 | **dr10** | 1.85 ± 1.01 | **dr15** | 3.92 ± 2.13 |
| $D_{KLR}$ | 0.48 | | | | |

**Table 4**
The results of the $D_{KL_N} \pm \sigma(D_{KL_N})$ measure between the LFD probability distributions of glaucomatous retinas from the HRF dataset and the mean probability distribution of healthy retinas from the same dataset.

| $D_{KL_N} \pm \sigma(D_{KL_N})$ | | | | | |
|---|---|---|---|---|---|
| **g1** | 4.95 ± 2.69 | **g6** | 3.14 ± 1.71 | **g11** | 3.63 ± 1.97 |
| **g2** | 4.06 ±2.20 | **g7** | 5.58 ± 3.03 | **g12** | 3.36 ± 1.83 |
| **g3** | 6.22 ± 3.38 | **g8** | 5.10 ± 2.77 | **g13** | 6.36 ± 3.45 |
| **g4** | 6.91 ± 3.75 | **g9** | 7.54 ± 4.09 | **g14** | 5.16 ± 2.80 |
| **g5** | 3.35 ± 1.82 | **g10** | 7.26 ± 3.95 | **g15** | 4.48 ±2.43 |
| $D_{KLR}$ | 0.48 | | | | |

of $D_{KL_N} \pm \sigma(D_{KL_N}) = 5.10 \pm 2.77$. As in the previous case, the LFD probability distribution curve shifts slightly towards low fractality compared to retina g12. In this retina, the low fractality increases, with a degree of affectation of 20.4 %, while high fractality decreases, with an AD of 25.7 %, as shown in Fig. 12.B. For the severe case, retina g1 was selected, which presents a value $D_{KL_N} \pm \sigma(D_{KL_N}) = 6.36 \pm 3.45$. In this case, the shift in the LFD distribution is even greater than the previous cases. As shown in Fig. 12.C, there is a very noticeable increase in the low-F, with an AD of 44.9 %, and a decrease in the high-F, with an AD of 16.6 %. Therefore, it is observed that in glaucoma cases, the vessels with low fractality, which correspond to the microvessels of the retina also increase as $D_{KL_N}$ increases, while the vessels with high fractality decrease.

As for the results of multifractal analysis, the mean multifractal spectra of the healthy, glaucoma and DR retina groups were first plotted to observe the multifractality behaviour of the pathological groups compared with the control group, as shown in Fig. 13. A notable difference is observed between the multifractal spectra of the pathological retinas (DR and glaucoma) and those of the healthy retinas. This difference is especially evident in the left side of the spectrum, which represents the multifractality.

The multifractal spectra of DR and glaucoma retinas show a greater variety of singularities with different fractal dimensions compared to healthy retinas, as seen in Fig. 13.

Furthermore, it is observed that DR group presents a slightly higher multifractal spectrum side than the glaucoma group and higher than the healthy retina group. To quantify the divergence between the spectra of pathological and healthy retinas, the MD1 and MD2 metrics were applied. The results of the MD1 and MD2 metrics for the characterization of the multifractal spectra of pathological retinas are shown in Tables 5 and 6.

With both metrics, it can be observed that the metric distances of these pathological retinas present different degrees of severity, allowing the retinas to be classified according to these distances as mild, moderate and severe. These retinas present the same degrees of severity in both measurement methods. Therefore, three cases of DR and glaucoma retinas with different degrees of severity are selected, and their multifractal spectra are shown in Fig. 14. This figure shows that the DR and glaucoma retina cases selected as mild (dr11 and g12), barely differ in their spectra from the average spectrum of the control group (healthy retinas). For the moderate cases (dr13 and g13), it can be observed that the spectra begin to diverge and show more distinction from the control group. In severe cases (dr1 and g15) the divergence between the pathological spectra and the control group is clearly visible.

In the case of the DR group, a mean MD1 distance of $d(\overline{DR}, R) = 1.61$ is obtained, where $R$ is the group of healthy retinas. As can be seen, this distance $d(\overline{DR}, R) > 1$, therefore, this indicates that the difference between both spectra is considered as a degree of pathology. In the case of the glaucoma group, a MD1 distance of $d(\overline{G}, R) = 1.47$ is obtained. As in the DR group, the difference between the mean spectra of the control and DR groups is significant, and at the same time it is smaller than the DR group. With respect to the MD2 metric, in the case of the DR group this distance is still higher in this group compared to the glaucoma group, which show a distance of $D(\overline{DR}, R) = 3.00$, and $D(\overline{G}, R) = 2.26$, respectively.

The results of the "MD3" metric, which measures the differences between the parameters α and f(α) that characterize the multifractal spectra of each group of retinas as a function of $q$, are shown in Fig. 15. When comparing the multifractal spectra of the DR and glaucoma groups against the control group, significant deviations are observed across the entire range of q. Specifically, differences manifest in both small-scale fluctuations ($q < 0$) and large-scale fluctuations ($q > 0$), as shown in Fig. 15.A. Although large fluctuations ($q > 0$) not only allow for better differentiation between healthy and pathological retinas but also help to distinguish between the two pathological groups (see Fig. 15.A).

In the case of DR, the results indicate that the differences between the retinas of this group and healthy retinas are observed above all in large fluctuations (q > 0) that represent strong singularities or multifractality. As for the glaucoma group, the difference is greater above all in small fluctuations (q < 0) that represent weak singularities or monofractality. The Kruskal-Wallis test indicates that the Mahalanobis distance of the parameter α between the DR and glaucoma groups compared to the control group is significant for large fluctuations (q > 0) (see Fig. 15.B). As for the parameter f(α), this distance is significant for small and large fluctuations, i.e. for both strong and weak singularities (see Fig. 15.C). This is evident from the area below the dotted line representing *p-value* $< 0.05$, indicating a greater region of statistically significant difference between the groups. These results demonstrate that the parameters α and f(α) are two characteristic parameters of multifractal spectra that can be used to characterize pathological retinas.

## 4. Discussion

In this study, a retinal image characterization method based on the measurement of the fractal dimension and the multifractal spectrum of the retinal vasculature has been developed. In this work, two types of fractal dimension measurement (Dlc and LFD) and different multifractal spectrum metrics have been explored and tested on different groups of retinas, both healthy and pathological. Both methods of fractal dimension measurement have shown their effectiveness in determining the FD of the retinal vasculature. However, the local fractal dimension (LFD) is more suitable for pathological retinas, since it presents a high SNR, which supports its stability in FD measurement. In addition, this measurement method has been widely used in the literature and has demonstrated its effectiveness in measurement [60–63]. Another metric

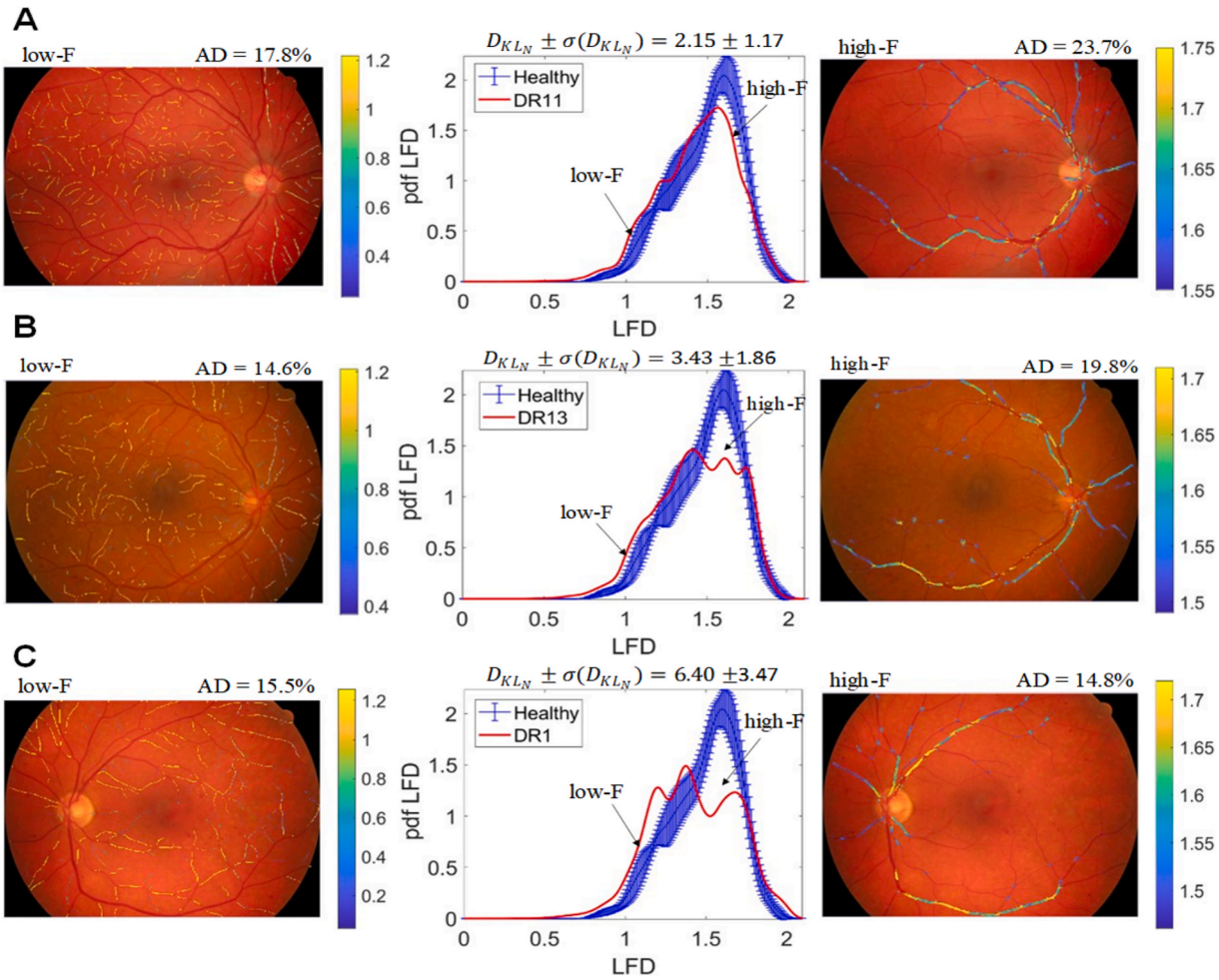


**Fig. 11.** (A) Representation of the points identified as abnormal in the retinal vasculature of the retina dr11 classified as mild according to the $D_{KL_N}$ value; (B) a moderate case, dr13; and (C) a severe case dr1.

that has been developed to determine the accuracy of the FD measurement is a measure based on the Wilcoxon rank-sum test. This metric has shown that the LFD measurement is more effective in distinguishing between healthy and pathological retinas. It has been used to characterize the pathological retinas by analysing the fractal dimension of their retinal vasculature. Based on this, an algorithm was developed that calculates the LFD probability distributions for each pathological retina and compares it to with the mean LFD probability distribution and the standard deviation of healthy retinas. This algorithm has made it possible to detect all regions considered anomalous or abnormal within the retinal vasculature and to assign a degree of severity to the detected pathology.

A Kullback-Leibler divergence distance metric has been used to quantify the degree of affectation in pathological retinal vasculature by measuring the distance between the LFD probability distributions of the pathological retinas and the mean LFD probability distribution of the healthy retinas. Both methods for characterizing and quantifying retinal pathology have shown good performance in detecting abnormalities in pathological retinas. In addition to providing a measure of abnormality, these metrics enable classification of the severity of the pathology based on the FD measurement.

In diabetic retinopathy (DR), the retinal vasculature undergoes progressive alterations that affect both its structure and vascular complexity. These changes begin in the early stages of the disease, such as in non-proliferative diabetic retinopathy (NPDR), where microaneurysms, hard exudates, haemorrhages, and venous beading typically occur [13], and progress further in more advanced stages, such as in proliferative diabetic retinopathy (PDR), characterized by neovascularization [15].

In the present study, our results showed that DR retinas, the LFD probability distribution indicates lower fractal dimension values as $D_{KL_N}$ increases. This decrease can be explained by multiple pathological mechanisms. The factors associated with the reduction of FD are diverse, some possible explanations can be associated with microangiopathy because diabetes causes direct damage to blood vessels, and this affects the structure and organization of the vascular network of the retina [64]. This loss of structural complexity is directly reflected in the reduction in FD.

A relevant question is to identify which specific alterations primarily contribute to this decrease. The images used showed several characteristic signs of DR, including neovascularization. Indeed, according to Odstrcilík et al. [51], the HRF dataset includes images with neovascular networks, haemorrhages, bright lesions, and laser-treated areas, indicating that many retinas present an advanced stage of the disease.

Neovascularization occurs in response to retinal ischemia, which in turn is a consequence of vascular damage induced by chronic hyperglycemia, and causes its occlusion, limiting blood flow. As a compensatory mechanism, the retina releases growth factors, such as vascular endothelial growth factor (VEGF), which promote the formation of new vessels [15]. However, these neovessels often have an anomalous and disorganized structure, lacking the hierarchical branching typical of the original vascular network. This structural disorganization contributes to a lower geometric complexity and, therefore, a reduction in fractal dimension. It is important to note that even before the development of

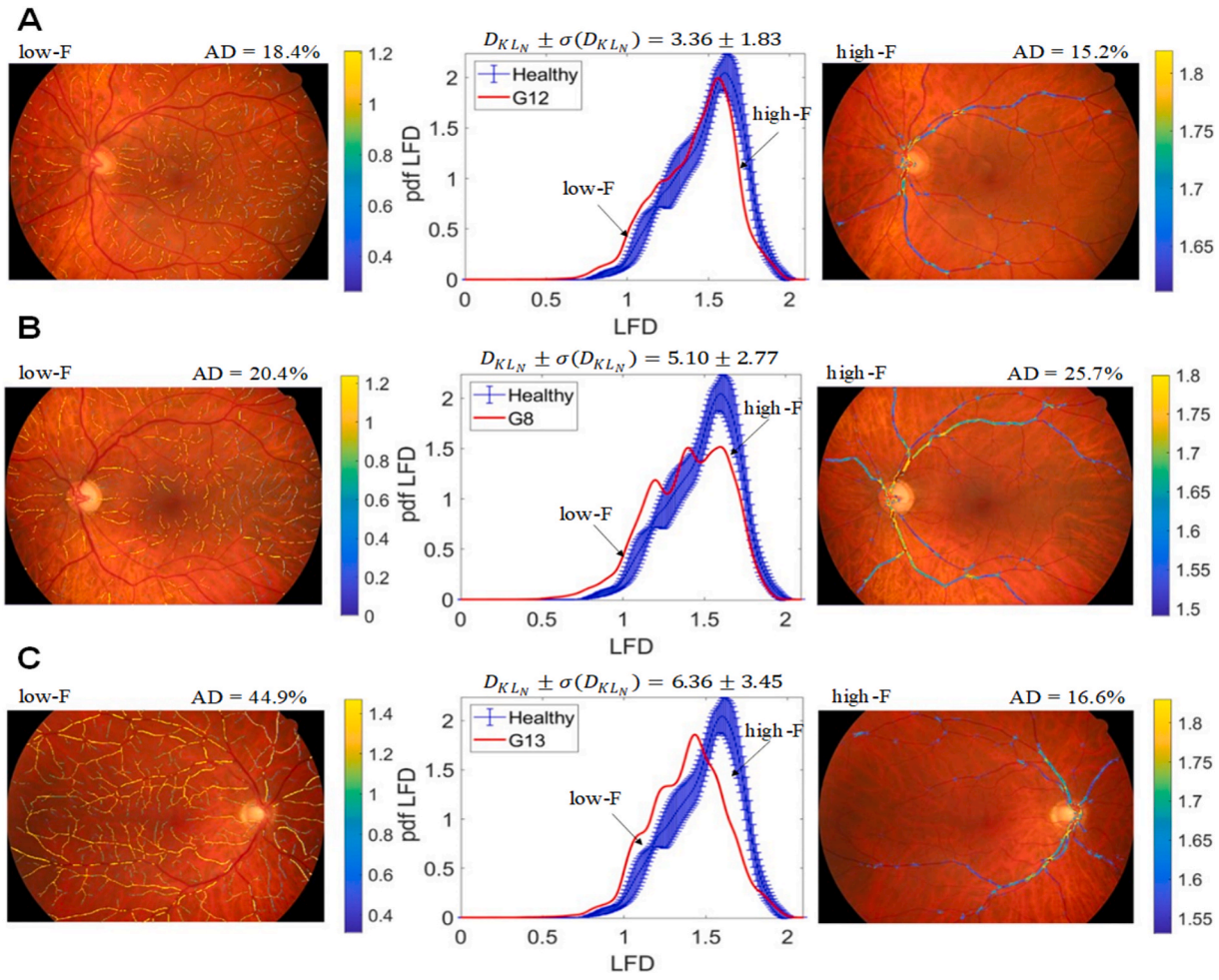


**Fig. 12.** Representation of the abnormal points of the retinal vasculature of a g12 glaucomatous retina classified as mild according to the $D_{KL_N}$ value; (B) a moderate case of a g8 glaucomatous retina; and (C) a case of a severe g13 retina.

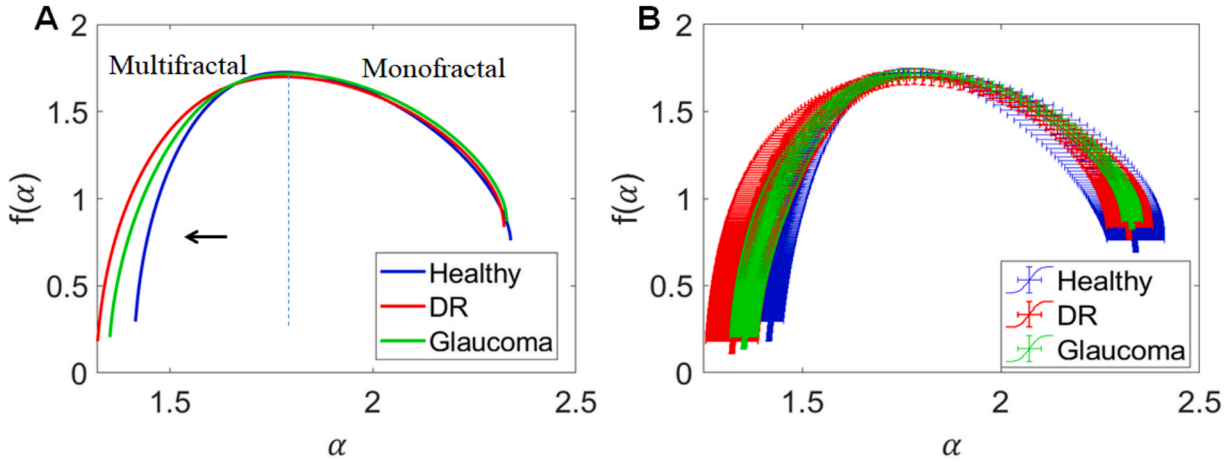


**Fig. 13.** (A) Representation of the mean multifractal spectra of the healthy retina group (blue), the glaucoma group (green) and DR (red). (B) Standard deviation of each spectrum (B).

neovessels, significant changes in vascular morphology are already evident in the non-proliferative stages [13], which could also contribute to the reduction of FD. Several studies have reported decreases in FD during NPDR, a stage characterized by microaneurysms, exudates, haemorrhages and intraretinal microvascular abnormality (IRMA), which reflect ischemic processes and morphological changes in the vascular network [16,65,66]. This means that even retinas not yet in the proliferative diabetic retinopathy (PDR) stage within this HFR dataset may exhibit a reduced fractal dimension.

Overall, the observed decrease in fractal dimension can be attributed to a combination of several pathological factors affecting vascular organization, both in early and advanced stages of the disease. These

**Table 5**
MD1 results for each DR retina and glaucoma from the HRF dataset, and the mean MD1 for each group.

| **MD1** $=d(p_i, R)$ | | | | | |
|---|---|---|---|---|---|
| **dr1** | 2.63 | **dr6** | 1.86 | **dr11** | 0.79 |
| **dr2** | 1.06 | **dr7** | 0.95 | **dr12** | 2.41 |
| **dr3** | 2.11 | **dr8** | 1.57 | **dr13** | 1.31 |
| **dr4** | 2.44 | **dr9** | 1.06 | **dr14** | 1.35 |
| **dr5** | 2.34 | **dr10** | 0.92 | **dr15** | 1.36 |
| $\overline{dr}$ | 1.61 | | | | |
| **g1** | 1.63 | **g6** | 1.26 | **g11** | 1.5647 |
| **g2** | 1.34 | **g7** | 1.40 | **g12** | 0.9065 |
| **g3** | 1.76 | **g8** | 1.6526 | **g13** | 1.7100 |
| **g4** | 1.09 | **g9** | 1.6191 | **g14** | 1.7102 |
| **g5** | 0.74 | **g10** | 1.3173 | **g15** | 2.3575 |
| $\overline{g}$ | 1.47 | | | | |

**Table 6**
MD2 results for each DR retina and glaucoma from the HRF dataset, and the mean MD2 for each group.

| MD2 $= D\ (p_i, R)$ | | | | | |
|---|---|---|---|---|---|
| **dr1** | 8.16 | **dr6** | 2.77 | **dr11** | 1.37 |
| **dr2** | 2.29 | **dr7** | 1.20 | **dr12** | 2.89 |
| **dr3** | 2.52 | **dr8** | 2.10 | **dr13** | 3.71 |
| **dr4** | 6.02 | **dr9** | 1.16 | **dr14** | 2.01 |
| **dr5** | 4.85 | **dr10** | 1.28 | **dr15** | 2.74 |
| $\overline{dr}$ | 3.00 | | | | |
| **g1** | 2.88 | **g6** | 1.81 | **g11** | 2.14 |
| **g2** | 2.24 | **g7** | 1.86 | **g12** | 1.34 |
| **g3** | 3.96 | **g8** | 2.03 | **g13** | 1.91 |
| **g4** | 1.57 | **g9** | 2.25 | **g14** | 1.24 |
| **g5** | 1.67 | **g10** | 2.21 | **g15** | 4.82 |
| $\overline{g}$ | 2.26 | | | | |

include ischemia, progressive structural damage to vessels, and the presence of neovascularization, all of which impair the complexity of retinal vascular architecture [23,24,67].

Some results consistent with the findings of this paper, Ţălu et al. [65] in their study of NPDR characterization by fractal analysis found that subtle changes in the fractal dimension occur at different stages of NPDR. They also found that in mild NPDR the fractal dimension is slightly higher than the corresponding values for normal images, while for moderate and severe cases the fractal dimension decreases with more severity in severe cases. Grauslund et al. [16] in their study of micro and macrovascular complications in type 1 diabetes they found that a lower fractal dimension of the retinal vasculature was related to PDR.

Other studies using different techniques for visualizing the retinal vasculature and analysing the fractal dimension of the same in different regions claim that the FD decreases in cases of DR. Among these studies, the study by Zahid et al. [17] of the analysis of the fractal dimension in eyes with DR using optical coherence tomography angiography (OCT-A) stands out. In this work, the authors demonstrated that the FD is significantly reduced in the superficial and deep capillary plexuses in eyes with DR.

Chen et al. [18] also use OCT-A to determine the capacity of the fractal dimension to detect early changes in the microvascular network of the retina in patients with type 2 diabetes. In this study, they observed that the FD of two capillary layers of the retina in most regions is significantly minimal in diabetic patients with DR. Avakian et al. [66] studied the FD of the macular region of normal and NPDR retinas, and obtained significantly higher FD in the normal macular region than in the NPDR macular region, while the paramacular areas were not very significant.

In contrast to the above studies, others found no significant difference between healthy and DR retinas [68–71], and others found high FD compared to healthy cases. Aliahmad et al. [72] that studied the FD of a group of 189 retinal images classified into DR retinas versus healthy retinas (control group) found that the FD of DR retinas have a higher FD value than control retinas. Another study of Cheung et al. [73] that analysed the FD in 729 patients with diabetic retinopathy with type 1 diabetes, obtained a result of high FD in cases of patients with diabetic retinopathy than healthy patients.

These last two studies have reported high FD values [72,73]; however, in our study, low FD was observed in cases of diabetic retinopathy (DR). Both studies used images of retinas with mild to moderate DR [73] or with no observable DR [72]. Therefore, this discrepancy could be due to several factors, including the inclusion of advanced cases, such as proliferative diabetic retinopathy (PDR). In these cases, as explained in previous sections, capillary loss and neovascularization can lead to a reduction in vascular complexity and, consequently, in FD.

Furthermore, in the study by Aliahmad et al. [72], the higher reported FD values could be related to clinical characteristics of the diabetic cases included. Specifically, only a minority presented with mild non-proliferative diabetic retinopathy (NPDR), while the majority showed no observable signs of DR. This could partly explain the higher FD observed, as the early or subclinical stages of the disease may not yet reflect the vascular rarefaction seen in more advanced DR.

In the case of glaucoma, our results showed reduced fractal dimension values. The etiology of glaucoma is still unknown. Indeed, it is not possible to attribute the decrease in fractal dimension to a single pathophysiological mechanism. Several factors could be involved.

The glaucomatous retinal images analysed in this study correspond to advanced stages of the disease, characterized by significant loss in the

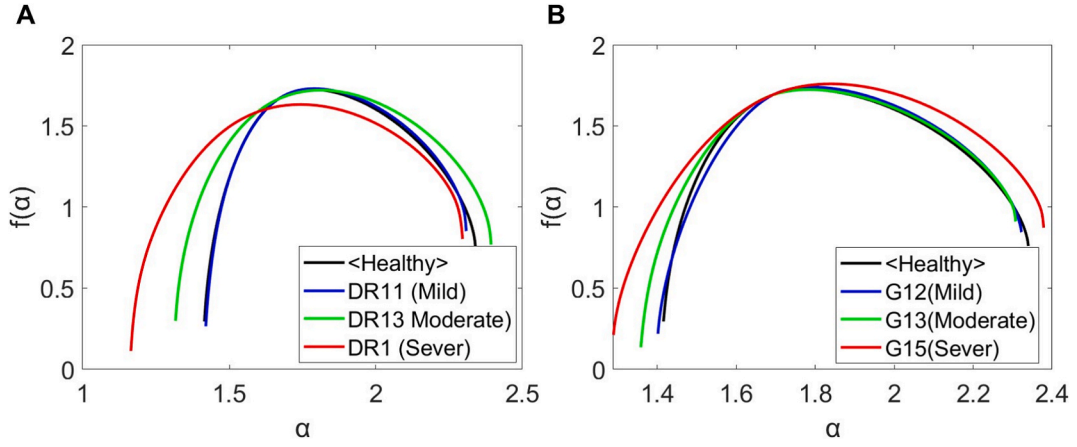


**Fig. 14.** (A) The mean multifractal spectrum of healthy retinas compared with multifractal spectra of three DR retinas classified as mild, moderate, and severe according to MD1-MD2 metrics, (B) three other cases of glaucoma retinas.

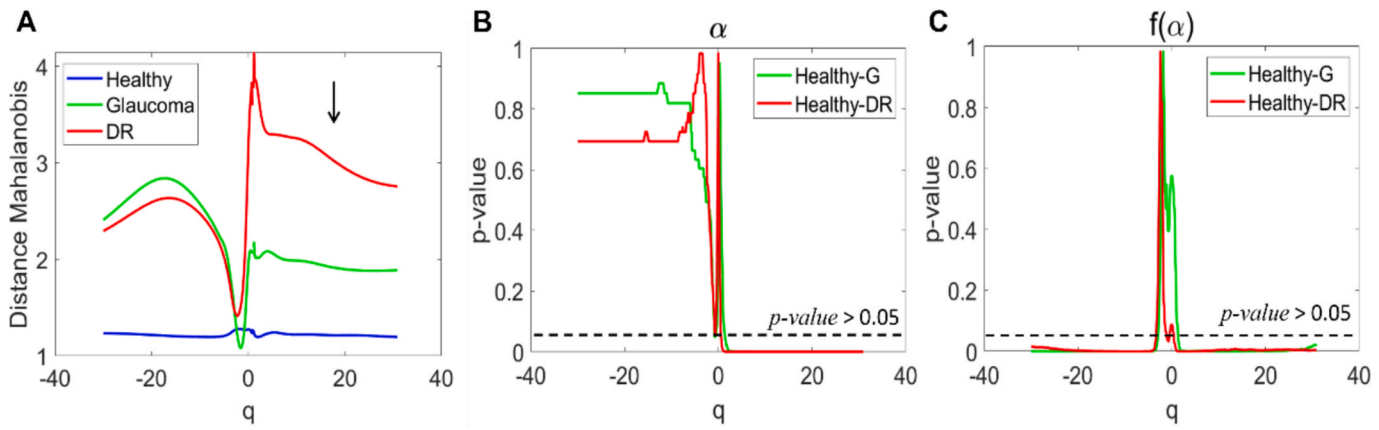


**Fig. 15.** Mahalanobis distance between the parameters α and f(α) characteristic of the multifractal spectra of the healthy, glaucoma and DR retina groups as a function of the parameter *q*. B) The results of the Kruskal-Wallis test for significant Mahalanobis distances (*p-value*) of the parameter α as a function of *q* for healthy retinas vs glaucoma and healthy retinas vs DR, C) the significant Mahalanobis distances (*p-value*) of the parameter f(α) as a function of *q*.

nerve fiber layer (RNFL). According to the article by Odstrcilík et al. [51], the images of patients with glaucoma in the HRF dataset correspond to advanced stages of the disease, showing signs of both focal and diffuse nerve fiber layer loss, which reflects significant structural damage.

Glaucoma has been associated with ocular blood flow dysfunction, particularly in the peripapillary and macular regions. This disturbance in perfusion is closely related to the loss of ganglion cells and their axons, which reduces the metabolic demand in affected areas. As a result, progressive hypoperfusion occurs, impacting the retinal capillaries. These events alter the vascular branching density, could be reflected in a reduction in fractal dimension as the disease progresses.

Therefore, this mechanism could explain the decrease in FD observed in our results, which is consistent with findings reported in the literature.

Other factors could be involved in the decreased fractal dimension. For example, ischemia affecting the optic nerve and different layers of the retina may reduce the supply of oxygen and nutrients, thereby altering the organization of the vascular network and reducing its geometric complexity [74].

Likewise, vascular remodeling processes can induce structural changes that manifest as a decreased FD [75]. Neural damage and ganglion cell apoptosis have also been proposed to affect the autoregulation of blood flow, which impacts the structure of the vascular network [76,77]. Finally, the inflammatory and immune response could directly influence the architecture of the retinal vessels, thus contributing to the changes observed in the fractal dimension [78].

Since multiple factors could be involved, it is not possible to determine with certainty which is primarily responsible for the reduction in FD. Furthermore, the objective of this study was not to identify the underlying biological causes of this phenomenon. As indicated in previous studies, there is still no definitive consensus on the vascular etiology of glaucoma.

Instead, our study focuses on providing quantitative metrics that characterize and describe the degree of vascular alteration present in the images, regardless of the specific biological mechanism that caused these alterations.

There are several clinical and population studies in the literature that have shown that changes in the retinal vasculature are related to a decrease in fractal dimension. These studies are associated with optic nerve damage and glaucoma. Some of the findings related to the decrease in FD in glaucoma are observed in [79,80]. These two studies have shown that there is a relationship between the vascular calibre of the retinal vessels and glaucoma, such that both tortuosity, branching angle and fractal dimension have smaller values in glaucomatous eyes than in healthy eyes. Other studies suggest that the FD in the optic nerve head is significantly reduced in advanced glaucoma and is correlated with optic disc damage, when, in the early stage of the disease, its value was similar to the FD of healthy eyes [30]. Ciancaglini et al. [80] found a relationship between ONH (optic nerve head) damage and a reduced fractal dimension of the retinal vasculature.

Wu et al. [79] in their study The Singapore Malay Eye Study reported results consistent with the findings obtained in this work, where they showed that low FD of retinal vasculature is a recurrent feature in glaucoma. Tham et al. [81] that examined the relationship between vascular geometry parameters such as calibre, tortuosity and fractal dimension with retinal nerve fibre layer (RNFL) and ganglion cell inner plexiform layer (GC-IPL) parameters using gradable retinal photography and OCT images and found an association between decreased FD, calibre and vascular tortuosity with glaucomatous retinas.

In this work, in addition to fractal analysis, multifractal analysis was also studied. In the multifractal analysis, the difference between the multifractal spectra of DR and glaucoma retinas in relation to healthy retinas was studied by analysing the different descriptive parameters of the multifractal spectrum. Using different metrics developed by the same authors, it was observed that there is a significant difference between the MFSs of the pathological groups and the healthy retinas. These metrics allow characterizing each of the pathological retinas and providing a quantification of their affectation.

Specifically, the multifractal spectrum becomes wider on its left side (multifractal) for the pathological retinas studied in this manuscript (glaucoma and diabetic retinopathy) compared to healthy retinas. The statistical tests used locate the significant difference in the parameter α, which measures local vascular irregularity. In this sense, diabetic retinopathy produces vessels with greater variability in irregularity than glaucoma and healthy retinas (see Fig. 13). It should be noted that, although various parameters of the multifractal spectrum (such as $\alpha$, $f(\alpha)$,$\Delta\alpha$,$\Delta f$, among others) have been extracted and analysed and used as a tool to characterize the spectrum of healthy retinas, DR and glaucoma, it has not been possible to establish a direct relationship between these and specific pathological characteristics, due to the lack of detailed clinical information in the dataset used. In the literature, these parameters have been mainly used to characterize the geometric complexity of the vascular network, without there being a clear biological interpretation of each of them so far. Therefore, their use in this work is aimed at quantitatively describing vascular morphology, rather than identifying specific pathophysiological mechanisms.

In this sense, future work could focus on studying the relationship between these parameters and the different characteristic alterations of diabetic retinopathy and glaucoma based on novel techniques. The preliminary results of the study in this manuscript demonstrate the usefulness of metrics based on the multifractal spectrum of the retinal

vasculature for characterizing pathologies, which opens the way for future research. Their implementation in larger dataset, combined with advanced segmentation techniques [82] and deep learning techniques [83–85] could strengthen the proposed method and advance the clinical utility of the metrics and the standardization of the proposed measurement methods.

Similar findings were obtained in other studies related to this topic. Relan & Khatter [86] used the same image dataset used in this study (HRF) to study the multifractal analysis of the three groups of retinal images: healthy, DR and glaucoma. The images were processed by segmentation and skeletonization. The authors determined significant differences between the spectra of the pathological and segmented healthy retinas. However, with the skeleton images they did not find any significant difference.

The authors of this work did not find any further studies in the literature that studied the multifractal analysis of these three groups of retinas, and the only study that was found, the results in principle agree with the findings obtained in this work.

The literature indicates that the retinal vasculature has a multifractal geometric architecture, therefore, a multifractal analysis provides an overview of the retinal vasculature regions at local and global levels [87,88]. There are several methods of multifractal analysis measurement among which the generalized multifractal dimension ($D_q$) is the most popular method in the literature. Moreover, the results reported in the literature depend on several factors such as the multifractal measurement method, the segmentation algorithms used as well as the different calculations used [8,89,90]. The descriptive parameters of the multifractal spectrum used in this study have been used in different topics in the literature to characterize multifractal spectra, [47,49,88], and their effectiveness in characterizing the analysed multifractal spectra has been determined.

## 5. Conclusions

In conclusion, in this work, fractal and multifractal analysis have been used to characterize pathological retinas in comparison with healthy retinas. Different metrics were used to characterize and provide a quantification of the pathological relevance of the retinas based on fractal measurements. One of the main novelties of this work is the use of metrics based on statistical distances, such as the Mahalanobis distance and the Kullback-Leiberg divergence, to not only characterize retinal vaculature pathology but also quantify the degree of pathology. This allows for the expansion of retinal classification from grade-based scales (ETDRS) to numerical scales through the development of new techniques for measuring the regularity of the retinal vasculature compared to healthy retinas. Particularly sensitive have been techniques based on the characterization of the shape of the multifractal spectrum, which allows for the identification of the parameter α as a relevant and highly variable factor between healthy and pathological retinas, at least in the study of glaucoma and diabetic retinopathy. The results were based on quantitative and qualitative measures and have managed to determine an agreement between the findings obtained in the literature.

This study has some limitations that should be considered when interpreting the results. First, the limited number of images used, especially of retinas with diabetic retinopathy and glaucoma, prevents the findings from being general enough. The study has to be taken as a first step in further research. This limitation is primarily due to two fundamental reasons established in previous studies by the same authors:

i. Manual segmentation (Gold Standard): In a previous study by the same authors [40], it was shown that some automatic segmentation methods can influence the calculation of the fractal and multifractal dimension. Therefore, in this work, manually segmented images (Gold Standard) have been used in order to minimize any bias introduced by the segmentation method and thus ensure greater reliability in the results.
ii. Uniformity in image acquisition: As demonstrated in the same previous study [40], differences in acquisition equipment significantly affect the calculation of the fractal dimension (FD) and the multifractal spectrum. Therefore, a dataset that ensures homogeneity in size, type of retinograph and capture conditions was selected: the HRF dataset, unique in the literature with images of healthy retinas, diabetic retinopathy and glaucoma, all captured with the same device, and presents manually segmented images.

Another important limitation is the lack of detailed clinical classification of pathological images. The images are not divided by disease stage or annotated with specific characteristics, making it difficult to establish a direct relationship between the multifractal findings and the pathological factors responsible for the abnormalities observed in DR and glaucoma.

Finally, another limitation is the reliance on manual segmentation, as mentioned above, which, while accurate, limits the data volume. Future studies hope to implement more advanced artificial intelligence-based segmentation methods, previously validated as interchangeable with manual segmentation, to expand the dataset without compromising the quality of the measurements [40].

For future work, we plan to acquire a larger number of images classified and annotated by experts, or using automatic classification techniques based on deep learning, which will allow for a more precise study of the association between the different parameters of the multifractal spectrum and the characteristic clinical and structural aspects of these pathologies.

## CRediT authorship contribution statement

**Asmae Igalla El-Youssfi:** Writing – review & editing, Writing – original draft, Software, Methodology, Investigation, Formal analysis, Conceptualization. **José Manuel López-Alonso:** Writing – review & editing, Writing – original draft, Validation, Supervision, Software, Methodology, Formal analysis, Conceptualization.

## Declaration of competing interest

The authors declare that they have no known competing financial interest or personal relationship that could influence the work reported in this paper.

## Acknowledgement

This research was developed thanks to the predoctoral grant awarded by the Complutense University of Madrid and Banco Santander [reference number CT82/20-CT83/20].

## Data availability

Data will be made available on request.

## References

[1] A. Rehfeld, M. Nylander, K. Karnov, The cardiovascular system, in: A. Rehfeld, M. Nylander, K. Karnov (Eds.), Compendium of Histology: A Theoretical and Practical Guide, Springer International Publishing, Cham, 2017, pp. 315–350, https://doi.org/10.1007/978-3-319-41873-5_17.
[2] A. Mitchell, B. Hill, The vascular system and associated disorders, Br. J. Nurs. 32 (2023) 718–724, https://doi.org/10.12968/bjon.2023.32.15.718.
[3] W.D. Strain, P.M. Paldánius, Diabetes, cardiovascular disease and the microcirculation, Cardiovasc. Diabetol. 17 (2018) 57, https://doi.org/10.1186/s12933-018-0703-2.
[4] F.D. Fuchs, P.K. Whelton, High blood pressure and cardiovascular disease, Hypertension 75 (2020) 285–292, https://doi.org/10.1161/HYPERTENSIONAHA.119.14240.

[5] Y. Wu, Y. Xiong, P. Wang, R. Liu, X. Jia, Y. Kong, F. Li, C. Chen, X. Zhang, Y. Zheng, Risk factors of cardiovascular and cerebrovascular diseases in young and middle-aged adults: a meta-analysis, Medicine (Baltimore) 101 (2022) e32082, https://doi.org/10.1097/MD.0000000000032082.
[6] A. Grzybowski, K. Jin, J. Zhou, X. Pan, M. Wang, J. Ye, T.Y. Wong, Retina fundus photograph-based artificial intelligence algorithms in medicine: a systematic review, Ophthalmol Ther. 13 (2024) 2125–2149, https://doi.org/10.1007/s40123-024-00981-4.
[7] R. Lopes, N. Betrouni, Fractal and multifractal analysis: a review, Med. Image Anal. 13 (2009) 634–649, https://doi.org/10.1016/j.media.2009.05.003.
[8] Ş. Ţălu, S. Giovanzana, Fractal and multifractal analysis of human retinal vascular network: a review, Human Veterin. Med. 3 (2011) 205–212.
[9] S. Yu, V. Lakshminarayanan, Fractal dimension and retinal pathology: a meta-analysis, Appl. Sci. 11 (2021) 2376, https://doi.org/10.3390/app11052376.
[10] T.P.H. Lin, Y.M. Wang, K. Ho, C.Y.K. Wong, P.P. Chan, M.O.M. Wong, N.C.Y. Chan, F. Tang, A. Lam, D.Y.L. Leung, T.Y. Wong, C.-Y. Cheng, C.Y. Cheung, C.C. Tham, Global assessment of arteriolar, venular and capillary changes in normal tension glaucoma, Sci. Rep. 10 (2020) 19222, https://doi.org/10.1038/s41598-020-75784-1.
[11] J. Lechner, O.E. O'Leary, A.W. Stitt, The pathology associated with diabetic retinopathy, Vis. Res. 139 (2017) 7–14, https://doi.org/10.1016/j.visres.2017.04.003.
[12] T.Y. Wong, T.-E. Tan, The diabetic retinopathy "pandemic" and evolving global strategies: the 2023 friedenwald lecture, Invest. Ophthalmol. Vis. Sci. 64 (2023) 47, https://doi.org/10.1167/iovs.64.15.47.
[13] D. Danek, B. Larsen, S. Anderson-Nelson, Non-proliferative diabetic retinopathy, Dis. Mon. 67 (2021) 101139, https://doi.org/10.1016/j.disamonth.2021.101139.
[14] R.S. Eshaq, A.M.Z. Aldalati, J.S. Alexander, N.R. Harris, Diabetic retinopathy: breaking the barrier, Pathophysiology 24 (2017) 229–241, https://doi.org/10.1016/j.pathophys.2017.07.001.
[15] S. Chaudhary, J. Zaveri, N. Becker, Proliferative diabetic retinopathy (PDR), Dis. Mon. 67 (2021) 101140, https://doi.org/10.1016/j.disamonth.2021.101140.
[16] J. Grauslund, A. Green, R. Kawasaki, L. Hodgson, A.K. Sjølie, T.Y. Wong, Retinal vascular fractals and microvascular and macrovascular complications in type 1 diabetes, Ophthalmology 117 (2010) 1400–1405, https://doi.org/10.1016/j.ophtha.2009.10.047.
[17] S. Zahid, R. Dolz-Marco, K.B. Freund, C. Balaratnasingam, K. Dansingani, F. Gilani, N. Mehta, E. Young, M.R. Klifto, B. Chae, L.A. Yannuzzi, J.A. Young, Fractal dimensional analysis of optical coherence tomography angiography in eyes with diabetic retinopathy, Invest. Ophthalmol. Vis. Sci. 57 (2016) 4940, https://doi.org/10.1167/iovs.16-19656.
[18] Q. Chen, Q. Ma, C. Wu, F. Tan, F. Chen, Q. Wu, R. Zhou, X. Zhuang, F. Lu, J. Qu, M. Shen, Macular vascular fractal dimension in the deep capillary layer as an early indicator of microvascular loss for retinopathy in type 2 diabetic patients, Invest. Ophthalmol. Vis. Sci. 58 (2017) 3785, https://doi.org/10.1167/iovs.17-21461.
[19] R.B. Forster, E.S. Garcia, A.J. Sluiman, S.M. Grecian, S. McLachlan, T. J. MacGillivray, M.W.J. Strachan, J.F. Price, Edinburgh Type 2 Diabetes Study (ET2DS) investigators, retinal venular tortuosity and fractal dimension predict incident retinopathy in adults with type 2 diabetes: the edinburgh type 2 diabetes study, Diabetologia 64 (2021) 1103–1112, https://doi.org/10.1007/s00125-021-05388-5.
[20] S. Bhardwaj, E. Tsui, S. Zahid, E. Young, N. Mehta, S. Agemy, P. Garcia, R.B. Rosen, J.A. Young, Value of fractal analysis of optical coherence tomography angiography in various stages of diabetic retinopathy, Retina 38 (2018) 1816–1823, https://doi.org/10.1097/IAE.0000000000001774.
[21] Y. Wu, M. He, W. Huang, W. Wang, Associations between retinal microvascular flow, geometry, and progression of diabetic retinopathy in type 2 diabetes: a 2-year longitudinal study, Acta Diabetol. 61 (2024) 195–204, https://doi.org/10.1007/s00592-023-02194-w.
[22] F. Family, B.R. Masters, D.E. Platt, Fractal pattern formation in human retinal vessels, Physica D 38 (1989) 98–103, https://doi.org/10.1016/0167-2789(89)90178-4.
[23] A.S. Al-Kharashi, Role of oxidative stress, inflammation, hypoxia and angiogenesis in the development of diabetic retinopathy, Saudi J. Ophthalmol. 32 (2018) 318–323, https://doi.org/10.1016/j.sjopt.2018.05.002.
[24] A. Aouiss, D. Anka Idrissi, M. Kabine, Y. Zaid, Update of inflammatory proliferative retinopathy: ischemia, hypoxia and angiogenesis, Curr. Res. Transl. Med. 67 (2019) 62–71, https://doi.org/10.1016/j.retram.2019.01.005.
[25] D. An, E. Chandrasekera, D.-Y. Yu, C. Balaratnasingam, Non-proliferative diabetic retinopathy is characterized by nonuniform alterations of peripapillary capillary networks, Invest. Ophthalmol. Vis. Sci. 61 (2020) 39, https://doi.org/10.1167/iovs.61.4.39.
[26] P.L. Nesper, P.K. Roberts, A.C. Onishi, H. Chai, L. Liu, L.M. Jampol, A.A. Fawzi, Quantifying microvascular abnormalities with increasing severity of diabetic retinopathy using optical coherence tomography angiography, Invest. Ophthalmol. Vis. Sci. 58 (2017) BIO307–BIO315, https://doi.org/10.1167/iovs.17-21787.
[27] G. Dimitrova, E. Chihara, Implication of deep-vascular-layer alteration detected by optical coherence tomography angiography for the pathogenesis of diabetic retinopathy, Ophthalmologica 241 (2019) 179–182, https://doi.org/10.1159/000495624.
[28] J. Phu, S.K. Khuu, A. Agar, I. Domadious, A. Ng, M. Kalloniatis, Visualizing the consistency of clinical characteristics that distinguish healthy persons, glaucoma suspect patients, and manifest glaucoma patients, Ophthalmol. Glaucoma. 3 (2020) 274–287, https://doi.org/10.1016/j.ogla.2020.04.009.
[29] T. Nishida, S. Moghimi, A.C. Chang, E. Walker, J.M. Liebmann, M.A. Fazio, C. A. Girkin, L.M. Zangwill, R.N. Weinreb, Association of intraocular pressure with retinal nerve fiber layer thinning in patients with glaucoma, JAMA Ophthalmol. (2022) e224462, https://doi.org/10.1001/jamaophthalmol.2022.4462.
[30] K.K.W. Chan, F. Tang, C.C.Y. Tham, A.L. Young, C.Y. Cheung, Retinal vasculature in glaucoma: a review, BMJ Open Ophth. 1 (2017) e000032, https://doi.org/10.1136/bmjophth-2016-000032.
[31] C.H. Song, S.H. Kim, K.M. Lee, Fractal dimension of peripapillary vasculature in primary open- angle glaucoma, Korean J. Ophthalmol. 36 (2022) 518–526, https://doi.org/10.3341/kjo.2022.0089.
[32] Q. Chen, S. Miao, Y. Jiang, D. Shi, W. You, L. Liu, M. Yusufu, Y. Chen, R. Wang, Associations of retinal microvascular density and fractal dimension with glaucoma: a prospective study from UK biobank, Ophthalmol. Sci. 5 (2025) 100661, https://doi.org/10.1016/j.xops.2024.100661.
[33] C. Chiquet, O. Gavard, L. Arnould, T. Mautuit, T.J. Macgillivray, A.M. Bron, R. Semecas, E. Trucco, A. Florent, Retinal vessel phenotype in patients with primary open-angle glaucoma, Acta Ophthalmol. 98 (2020) e88–e93, https://doi.org/10.1111/aos.14192.
[34] S. Banerjee, D. Easwaramoorthy, A. Gowrisankar, Mathematical background of deterministic fractals, in: S. Banerjee, D. Easwaramoorthy, A. Gowrisankar (Eds.), Fractal Functions, Dimensions and Signal Analysis, Springer International Publishing, Cham, 2021, pp. 1–19, https://doi.org/10.1007/978-3-030-62672-3_1.
[35] F. Huang, B. Dashtbozorg, J. Zhang, E. Bekkers, S. Abbasi-Sureshjani, T.T.J. M. Berendschot, B.M. ter Haar Romeny, Reliability of using retinal vascular fractal dimension as a biomarker in the diabetic retinopathy detection, J. Ophthalmol. (2016) 1–13, https://doi.org/10.1155/2016/6259047.
[36] F. Huang, J. Zhang, E.J. Bekkers, B. Dashtbozorg, B.M. ter Haar Romeny, Stability analysis of fractal dimension in retinal vasculature, in: Proceedings of the Ophthalmic Medical Image Analysis Second International Workshop, University of Iowa, Munich, Germany, 2015, pp. 1–8. doi: 10.17077/omia.1020.
[37] R. Wang, A.K. Singh, S.R. Kolan, E. Tsotsas, Fractal analysis of aggregates: correlation between the 2D and 3D box-counting fractal dimension and power law fractal dimension, Chaos, Solit. Fract. 160 (2022) 112246, https://doi.org/10.1016/j.chaos.2022.112246.
[38] X. Lyu, P. Jajal, M.Z. Tahir, S. Zhang, Fractal dimension of retinal vasculature as an image quality metric for automated fundus image analysis systems, Sci. Rep. 12 (2022) 11868, https://doi.org/10.1038/s41598-022-16089-3.
[39] M. Manera, L. Giari, J.A. De Pasquale, B. Sayyaf Dezfuli, Local connected fractal dimension analysis in gill of fish experimentally exposed to toxicants, Aquat. Toxicol. 175 (2016) 12–19, https://doi.org/10.1016/j.aquatox.2016.03.011.
[40] A.I. El-Youssfi, J.M. López-Alonso, Metrics for comparison of image dataset and segmentation methods for fractal analysis of retinal vasculature, Biomed. Signal Process. Control 105 (2025) 107650, https://doi.org/10.1016/j.bspc.2025.107650.
[41] O. Sijilmassi, J.-M. López Alonso, A. Del Río Sevilla, M. del C. Barrio Asensio, Multifractal analysis of embryonic eye tissues from female mice with folic acid deficiency. Part II: Local connected fractal dimension analysis, Chaos, Solitons Fract. 138 (2020) 109887, https://doi.org/10.1016/j.chaos.2020.109887.
[42] Ş. Ţălu, S. Stach, D.M. Călugăru, C.A. Lupaşcu, S.D. Nicoară, Analysis of normal human retinal vascular network architecture using multifractal geometry, Int. J. Ophthalmol. 10 (2017) 434–438, https://doi.org/10.18240/ijo.2017.03.17.
[43] R. Lopes, Multifractal analysis in neuroimaging, in: A. Di Ieva (Ed.), The Fractal Geometry of the Brain, Springer International Publishing, Cham, 2024, pp. 79–93, https://doi.org/10.1007/978-3-031-47606-8_4.
[44] A. Chhabra, R.V. Jensen, Direct determination of the f(alpha) singularity spectrum, Phys. Rev. Lett. 62 (1989) 1327–1330, https://doi.org/10.1103/PhysRevLett.62.1327.
[45] H. Salat, R. Murcio, E. Arcaute, Multifractal methodology, Physica A 473 (2017) 467–487, https://doi.org/10.1016/j.physa.2017.01.041.
[46] D. de Souza Santos, L.C.B. dos Santos, A. de Albuquerque Tavares, J.C. Carvalho, C. Leão, T. Delrieux, B.S. Stosic, Multifractal spectrum and lacunarity as measures of complexity of osseointegration, Clin. Oral Invest. 20 (2016) 1271–1278, https://doi.org/10.1007/s00784-015-1606-1.
[47] O. Bouzeboudja, B. Haddad, A. Taleb-Ahmed, S. Ameur, M. El Hassouni, Rachid Jennane, Multifractal analysis for improved osteoporosis classification, Biomed. Signal Process. Control 80 (2023) 104225, https://doi.org/10.1016/j.bspc.2022.104225.
[48] A. Biswas, H.P. Cresswell, C.S. Bing, A. Biswas, H.P. Cresswell, C.S. Bing, Application of multifractal and joint multifractal analysis in examining soil spatial variation a review, in: Fractal Analysis and Chaos in Geosciences, IntechOpen, 2012, https://doi.org/10.5772/51437.
[49] O. Sijilmassi, J.-M. López Alonso, A. Del Río Sevilla, M. del C. Barrio Asensio, Multifractal analysis of embryonic eye structures from female mice with dietary folic acid deficiency. Part I: Fractal dimension, lacunarity, divergence, and multifractal spectrum, Chaos, Solit. Fract. 138 (2020) 109885, https://doi.org/10.1016/j.chaos.2020.109885.
[50] A. Budai, R. Bock, A. Maier, J. Hornegger, G. Michelson, Robust vessel segmentation in fundus images, Int. J. Biomed. Imag. 2013 (2013) 154860, https://doi.org/10.1155/2013/154860.
[51] J. Odstrcilik, R. Kolar, A. Budai, J. Hornegger, J. Jan, J. Gazarek, T. Kubena, P. Cernosek, O. Svoboda, E. Angelopoulou, Retinal vessel segmentation by improved matched filtering: evaluation on a new high-resolution fundus image database, IET Image Proc. 7 (2013) 373–383, https://doi.org/10.1049/iet-ipr.2012.0455.
[52] C.A. Schneider, W.S. Rasband, K.W. Eliceiri, NIH image to ImageJ: 25 years of image analysis, Nat. Methods 9 (2012) 671–675, https://doi.org/10.1038/nmeth.2089.
[53] ImageJ, (n.d.). https://imagej.net/ij/ (Accessed June 14, 2025).

[54] A. Karperien, FracLac for ImageJ, NIH (2013), https://doi.org/10.13140/2.1.4775.8402.
[55] G. Landini, J.W. Rippin, How important is tumour shape? quantification of the epithelial-connective tissue interface in oral lesions using local connected fractal dimension analysis, J. Pathol. 179 (1996) 210–217, https://doi.org/10.1002/(SICI)1096-9896(199606)179:2<210::AID-PATH560>3.0.CO;2-T.
[56] G. Landini, P.I. Murray, G.P. Misson, Local connected fractal dimensions and lacunarity analyses of 60 degrees fluorescein angiograms, Invest. Ophthalmol. Vis. Sci. 36 (1995) 2749–2755.
[57] ranksum - Wilcoxon rank sum test - MATLAB, (n.d.). https://es.mathworks.com/help/stats/ranksum.html (Accessed June 12, 2025).
[58] F. Perez-Cruz, Kullback-Leibler divergence estimation of continuous distributions, in: IEEE International Symposium on Information Theory, 2008, pp. 1666–1670, https://doi.org/10.1109/ISIT.2008.4595271.
[59] kruskalwallis - Kruskal-Wallis test - MATLAB, (n.d.). https://es.mathworks.com/help/stats/kruskalwallis.html (Accessed June 12, 2025).
[60] M. Häfner, T. Tamaki, S. Tanaka, A. Uhl, G. Wimmer, S. Yoshida, Local fractal dimension based approaches for colonic polyp classification, Med. Image Anal. 26 (2015) 92–107, https://doi.org/10.1016/j.media.2015.08.007.
[61] K.W. Ketipearachchi, J. Tatsumi, Local fractal dimensions and multifractal analysis of the root system of legumes, Plant Prod. Sci. 3 (2000) 289–295, https://doi.org/10.1626/pps.3.289.
[62] H. Taud, J.-F. Parrot, Measurement of DEM roughness using the local fractal dimension, Géomorphol.: Relief Process. Environ. 11 (2005) 327–338, https://doi.org/10.4000/geomorphologie.622.
[63] S.G.K. Gadde, N. Anegondi, D. Bhanushali, L. Chidambara, N.K. Yadav, A. Khurana, A. Sinha Roy, Quantification of vessel density in retinal optical coherence tomography angiography images using local fractal dimension, Invest. Ophthalmol. Vis. Sci. 57 (2016) 246–252, https://doi.org/10.1167/iovs.15-18287.
[64] Diabetic Microangiopathy - an overview | ScienceDirect Topics, (n.d.). https://www-sciencedirect-com.bucm.idm.oclc.org/topics/medicine-and-dentistry/diabetic-microangiopathy (Accessed December 27, 2023).
[65] Ş. Ţălu, D.M. Călugăru, C.A. Lupaşcu, Characterisation of human non-proliferative diabetic retinopathy using the fractal analysis, Int. J. Ophthalmol. 8 (2015) 770–776, https://doi.org/10.3980/j.issn.2222-3959.2015.04.23.
[66] A. Avakian, R.E. Kalina, E. Helene Sage, A.H. Rambhia, K.E. Elliott, E.L. Chuang, J. I. Clark, J.-N. Hwang, P. Parsons-Wingerter, Fractal analysis of region-based vascular change in the normal and non-proliferative diabetic retina, Curr. Eye Res. 24 (2002) 274–280, https://doi.org/10.1076/ceyr.24.4.274.8411.
[67] M. Lin, Y. Chen, J. Jin, Y. Hu, K.K. Zhou, M. Zhu, Y.-Z. Le, J. Ge, R.S. Johnson, J.-X. Ma, Ischaemia-induced retinal neovascularisation and diabetic retinopathy in mice with conditional knockout of hypoxia-inducible factor-1 in retinal Müller cells, Diabetologia 54 (2011) 1554–1566, https://doi.org/10.1007/s00125-011-2081-0.
[68] S.W. Lim, N. Cheung, J.J. Wang, K.C. Donaghue, G. Liew, F.M.A. Islam, A. J. Jenkins, T.Y. Wong, Retinal vascular fractal dimension and risk of early diabetic retinopathy: a prospective study of children and adolescents with type 1 diabetes, Diabetes Care 32 (2009) 2081–2083, https://doi.org/10.2337/dc09-0719.
[69] C.-Y.-L. Cheung, E. Lamoureux, M.K. Ikram, M.B. Sasongko, J. Ding, Y. Zheng, P. Mitchell, J.J. Wang, T.Y. Wong, Retinal vascular geometry in Asian persons with diabetes and retinopathy, J. Diabetes Sci. Technol. 6 (2012) 595–605, https://doi.org/10.1177/193229681200600315.
[70] J.W.Y. Yau, R. Kawasaki, F.M.A. Islam, J. Shaw, P. Zimmet, J.J. Wang, T.Y. Wong, Retinal fractal dimension is increased in persons with diabetes but not impaired glucose metabolism: the Australian Diabetes, Obesity and Lifestyle (AusDiab) study, Diabetologia 53 (2010) 2042–2045, https://doi.org/10.1007/s00125-010-1811-z.
[71] T. Nagaoka, A. Yoshida, Relationship between retinal fractal dimensions and retinal circulation in patients with type 2 diabetes mellitus, Curr. Eye Res. 38 (2013) 1148–1152, https://doi.org/10.3109/02713683.2013.805232.
[72] B. Aliahmad, D.K. Kumar, M.G. Sarossy, R. Jain, Relationship between diabetes and grayscale fractal dimensions of retinal vasculature in the Indian population, BMC Ophthalmol. 14 (2014) 152, https://doi.org/10.1186/1471-2415-14-152.
[73] N. Cheung, K.C. Donaghue, G. Liew, S.L. Rogers, J.J. Wang, S.-W. Lim, A. J. Jenkins, W. Hsu, M.L. Lee, T.Y. Wong, Quantitative assessment of early diabetic retinopathy using fractal analysis, Diabetes Care 32 (2009) 106–110, https://doi.org/10.2337/dc08-1233.
[74] A.P. Cherecheanu, G. Garhofer, D. Schmidl, R. Werkmeister, L. Schmetterer, Ocular perfusion pressure and ocular blood flow in glaucoma, Curr. Opin. Pharmacol. 13 (2013) 36–42, https://doi.org/10.1016/j.coph.2012.09.003.
[75] X. Wang, M. Wang, H. Liu, K. Mercieca, J. Prinz, Y. Feng, V. Prokosch, The association between vascular abnormalities and glaucoma—what comes first? Int. J. Mol. Sci. 24 (2023) 13211, https://doi.org/10.3390/ijms241713211.
[76] R.W. Nickells, Apoptosis of retinal ganglion cells in glaucoma: an update of the molecular pathways involved in cell death, Surv. Ophthalmol. 43 (1999) S151–S161, https://doi.org/10.1016/S0039-6257(99)00029-6.
[77] R.H. Farkas, C.L. Grosskreutz, Apoptosis, neuroprotection, and retinal ganglion cell death: an overview, Int. Ophthalmol. Clin. 41 (2001) 111.
[78] G. Siasos, D. Tousoulis, G. Siasou, M.M. Moschos, E. Oikonomou, M. Zaromitidou, G. Marinos, P. Korompelis, A.G. Papavassiliou, C. Stefanadis, The association between glaucoma, vascular function and inflammatory process, Int. J. Cardiol. 146 (2011) 113–115, https://doi.org/10.1016/j.ijcard.2010.09.083.
[79] R. Wu, C.-Y.-L. Cheung, S.M. Saw, P. Mitchell, T. Aung, T.Y. Wong, Retinal vascular geometry and glaucoma: the Singapore Malay eye study, Ophthalmology 120 (2013) 77–83, https://doi.org/10.1016/j.ophtha.2012.07.063.
[80] M. Ciancaglini, G. Guerra, L. Agnifili, R. Mastropasqua, V. Fasanella, M. Cinelli, C. Costagliola, L. Ambrosone, Fractal dimension as a new tool to analyze optic nerve head vasculature in primary open angle glaucoma, In Vivo 29 (2015) 273–279.
[81] Y.-C. Tham, C.-Y. Cheng, Y. Zheng, T. Aung, T.Y. Wong, C.Y. Cheung, Relationship between retinal vascular geometry with retinal nerve fiber layer and ganglion cell-inner plexiform layer in nonglaucomatous eyes, Invest. Ophthalmol. Vis. Sci. 54 (2013) 7309–7316, https://doi.org/10.1167/iovs.13-12796.
[82] J. Wang, X. Li, Z. Ma, Multi-Scale Three-Path Network (MSTP-Net): a new architecture for retinal vessel segmentation, Measurement 250 (2025) 117100, https://doi.org/10.1016/j.measurement.2025.117100.
[83] Y. Zhao, X. Li, C. Zhou, H. Peng, Z. Zheng, J. Chen, W. Ding, A review of cancer data fusion methods based on deep learning, Inf. Fusion 108 (2024) 102361, https://doi.org/10.1016/j.inffus.2024.102361.
[84] L. Zhang, J. Wang, W. Wang, Z. Jin, Y. Su, H. Chen, Smart contract vulnerability detection combined with multi-objective detection, Comput. Netw. 217 (2022) 109289, https://doi.org/10.1016/j.comnet.2022.109289.
[85] M. Chen, W. Du, Dynamic relationship network and international management of enterprise supply chain by particle swarm optimization algorithm under deep learning, Exp. Syst. 41 (2024) e13081, https://doi.org/10.1111/exsy.13081.
[86] D. Relan, K. Khatter, Effectiveness of multi-fractal analysis in differentiating subgroups of retinal images, in: 2020 IEEE 17th India Council International Conference (INDICON), 2020, pp. 1–6, https://doi.org/10.1109/INDICON49873.2020.9342576.
[87] T. Stosic, B.D. Stosic, Multifractal analysis of human retinal vessels, IEEE Trans. Med. Imag. 25 (2006) 1101–1107, https://doi.org/10.1109/TMI.2006.879316.
[88] Int. J. Ophthalmol. (2017), https://doi.org/10.18240/ijo.2017.03.17.
[89] Ş. Ţălu, Characterization of retinal vessel networks in human retinal imagery using quantitative descriptors 5 (2013).
[90] M.Z.C. Azemin, D.K. Kumar, T.Y. Wong, J.J. Wang, P. Mitchell, R. Kawasaki, H. Wu, Age-related rarefaction in the fractal dimension of retinal vessel, Neurobiol. Aging 33 (194) (2012) e1–e4, https://doi.org/10.1016/j.neurobiolaging.2010.04.010.